JEM Journal of Experimental Medicine

BRIEF DEFINITIVE REPORT

Genetic manipulation of LKB1 elicits lethal metastatic prostate cancer

Ivana Hermanova[1*], Patricia Zúñiga-García[1*], Alfredo Caro-Maldonado[1], Sonia Fernandez-Ruiz[1,2], Fernando Salvador[2,3], Natalia Martín-Martín[1,2], Amaia Zabala-Letona[1,2], Marc Nuñez-Olle[3], Verónica Torrano[1,2,4], Laura Camacho[1,4], Jose M. Lizcano[5], Ana Talamillo[1], Suzanne Carreira[6], Bora Gurel[6], Ana R. Cortazar[1,2], Marc Guiu[3], Jose I. López[7], Anabel Martinez-Romero[2,8], Ianire Astobiza[1,2], Lorea Valcarcel-Jimenez[1], Mar Lorente[9], Amaia Arruabarrena-Aristorena[1], Guillermo Velasco[9,10], Antonio Gomez-Muñoz[4], Cristian Suárez-Cabrera[11,12], Iris Lodewijk[11,12], Juana M. Flores[13], James D. Sutherland[1], Rosa Barrio[1], Johann S. de Bono[6,14], Jesús M. Paramio[2,11,12], Jan Trka[15,16], Mariona Graupera[2,8], Roger R. Gomis[2,3,17], and Arkaitz Carracedo[1,2,4,18]

Gene dosage is a key defining factor to understand cancer pathogenesis and progression, which requires the development of experimental models that aid better deconstruction of the disease. Here, we model an aggressive form of prostate cancer and show the unconventional association of LKB1 dosage to prostate tumorigenesis. Whereas loss of *Lkb1* alone in the murine prostate epithelium was inconsequential for tumorigenesis, its combination with an oncogenic insult, illustrated by *Pten* heterozygosity, elicited lethal metastatic prostate cancer. Despite the low frequency of *LKB1* deletion in patients, this event was significantly enriched in lung metastasis. Modeling the role of LKB1 in cellular systems revealed that the residual activity retained in a reported kinase-dead form, LKB1^{K78I}, was sufficient to hamper tumor aggressiveness and metastatic dissemination. Our data suggest that prostate cells can function normally with low activity of LKB1, whereas its complete absence influences prostate cancer pathogenesis and dissemination.

Introduction

Prostate cancer (PCa) is primarily diagnosed as a localized disease that is considered curable with first-line therapies. However, two major limitations exist in its clinical management (Chang et al., 2014). First, a considerable proportion of men will relapse after such treatments. These patients will frequently fail to respond to subsequent lines of treatment (androgen pathway inhibitors and chemotherapy) and succumb to metastatic PCa. Second, a fraction of PCa patients will exhibit metastatic disease at diagnosis. Whereas the incidence of this phenomenon is estimated as <10% in populations heavily prescreened for prostate-specific antigen, it is thought to account for ≤50% of PCa mortality (James et al., 2015). The clinical management of lethal metastatic disease is the ultimate challenge in PCa. However, the success in recapitulating this phenomenon in experimental models has been limited (Arriaga and Abate-Shen, 2019).

LKB1 (the protein encoded by the gene *STK11*) is a master kinase with a prominent role as a tumor suppressor in various tissue types. This gene is mutated and deleted in lung, cervix, uterine, skin, and pancreatic cancers (Momcilovic and Shackelford, 2015). The study of LKB1 in cancer has been boosted by the development of mouse models with varying doses of the tumor suppressor, which result in a reduction of its levels of 50–100% (for heterozygous and homozygous knockout mice, respectively; Pearson et al., 2008) or 25–75% (through the combination of hypomorphic alleles with WT or knockout alleles, respectively; Huang et al., 2008).

[1]Center for Cooperative Research in Biosciences, Basque Research and Technology Alliance (BRTA), Derio, Spain; [2]CIBERONC (Centro de Investigación Biomédica en Red de Cáncer), Madrid, Spain; [3]Cancer Science Program, Institute for Research in Biomedicine, The Barcelona Institute of Science and Technology, Barcelona, Spain; [4]Biochemistry and Molecular Biology Department, University of the Basque Country, Bilbao, Spain; [5]Protein Kinases and Signal Transduction Laboratory, Institut de Neurociències and Departament de Bioquímica i Biologia Molecular, Universitat Autònoma de Barcelona, Bellaterra, Barcelona, Spain; [6]The Institute of Cancer Research, London, UK; [7]Department of Pathology, Cruces University Hospital, Biocruces Institute, University of the Basque Country, Barakaldo, Spain; [8]Vascular Signalling Laboratory, Program Against Cancer Therapeutic Resistance (ProCURE), Institut d'Investigació Biomèdica de Bellvitge, Barcelona, Spain; [9]Department of Biochemistry and Molecular Biology, School of Biology, Complutense University, Madrid, Spain; [10]Instituto de Investigaciones Sanitarias San Carlos, Madrid, Spain; [11]Grupo de Oncología Celular y Molecular, Hospital Universitario 12 de Octubre, Madrid, Spain; [12]Unidad de Oncología Molecular, Centro de Investigaciones Energéticas, Medioambientales y Tecnológicas, Madrid, Spain; [13]Department of Animal Medicine and Surgery, School of Veterinary Medicine, Complutense University of Madrid, Madrid, Spain; [14]The Royal Marsden National Health Service Foundation Trust, London, UK; [15]Childhood Leukaemia Investigation, Prague, Czech Republic; [16]Department of Paediatric Haematology/Oncology, Second Faculty of Medicine, Charles University and University Hospital Motol, Prague, Czech Republic; [17]Institució Catalana de Recerca i Estudis Avançats, Barcelona, Spain; [18]Ikerbasque, Basque Foundation for Science, Bilbao, Spain.

*I. Hermanova and P. Zúñiga-García contributed equally to this paper; Correspondence to Arkaitz Carracedo: acarracedo@cicbiogune.es.

© 2020 Hermanova et al. This article is distributed under the terms of an Attribution–Noncommercial–Share Alike–No Mirror Sites license for the first six months after the publication date (see http://www.rupress.org/terms/). After six months it is available under a Creative Commons License (Attribution–Noncommercial–Share Alike 4.0 International license, as described at https://creativecommons.org/licenses/by-nc-sa/4.0/).

Downloaded from http://rupress.org/jem/article-pdf/217/6/e20191787/1780008/jem_20191787.pdf by guest on 09 February 2026

Tumor suppressors are clinically and experimentally defined based on gene dosage. Knudson (1971) proposed that genes with such functions would follow the two-hit hypothesis, according to which cancer would emerge upon the loss of the second allele in cells with carrying a mutated gene. However, we know that the relationship between gene dosage and tumor-suppressive activity is more complex, which led to the introduction of concepts such as haploinsufficient tumor suppressors (Berger et al., 2011). However, further experimental effort is required for a comprehensive classification of tumor suppressors, based on evidence produced through the analysis of mouse models with hypomorphic alleles (Alimonti et al., 2010).

In this study, we generate an unprecedented model of lethal metastatic PCa by introducing perturbations in *Lkb1* in a precancerous setting and demonstrate the high competence of this kinase to suppress biological features of PCa.

Results and discussion

To ascertain the role of LKB1 in PCa, we engineered a series of *Lkb1* prostate-specific mutant mice based on a conditional mouse model (Fig. S1, A–D; see Materials and methods; Nardella et al., 2010; Pearson et al., 2008). The survival of mice with prostate-specific *Lkb1* ($Lkb1^{pc-/-}$) deficiency was indistinguishable from that of control counterparts (Fig. 1 A). Although *Lkb1* deletion led to increased tissue mass (Fig. S1 E), it did not result in any histological alteration (Fig. 1 B). These data are in contrast to results obtained using other Cre recombinases such as p450 CYP1A1-driven Cre, which show a broader tissue distribution in the urogenital track (Pearson et al., 2008). The discrepancies might be associated with the impact of the non-prostate epithelial deletion of *Lkb1* (Pearson et al., 2008). Also, the original description of this Cre driver reported expression in multiple tissues and cell types beyond the prostate (Ireland et al., 2004). Our results using a well-established prostate epithelium–restricted Cre driver support the notion that *Lkb1* loss is not an initiating event in prostate tumorigenesis.

Next, we evaluated whether deletion of *Lkb1* would contribute to PCa pathogenesis in the presence of an oncogenic event. To this end, we intercrossed prostate-conditional *Lkb1* knockout mice with a well-established driver of murine PCa, *Pten* knockout mice (Fig. S1, C and D). Whereas $Pten^{pc-/-}$ mice develop nonmetastatic PCa, the phenotype of heterozygous mice is limited to prostate intraepithelial neoplasia (PIN; Nardella et al., 2010). Surprisingly, the deletion of *Lkb1* resulted in a remarkable reduction in survival when combined with one allele deletion of *Pten* (Fig. 1 C). Since the combination of *Pten* heterozygosity with *Lkb1* loss (hereafter referred to as PTLK) resulted in early lethality, we performed histological characterization of all genotypes at 10 mo of age. PTLK mice exhibited PCa at full penetrance, whereas none of the other genotypes ($Pten^{pc+/-}$ $Lkb1^{pc+/+}$, $Pten^{pc+/-}$ $Lkb1^{pc+/-}$) presented lesions beyond PIN at the same age (Fig. 1 D). Moreover, the macroscopic and histopathological analysis of distant organs unexpectedly revealed that PTLK mice developed lung metastasis with an incidence >80% (justifying their reduced survival rate) and inguinal lymph node colonization to a lower extent (Fig. 1, E and F). Importantly, lung lesions were histologically identical to the prostatic tumor and exhibited positive staining for androgen receptor (AR), supporting the notion that the metastases were of prostatic origin (Fig. S1 F). No lesions were observed in heart, liver, spleen, kidney, or bone (Table S1).

PCa disseminates predominantly to bone. However, dissemination to lungs is well recognized to occur in 10–20% of metastatic disease (Arriaga and Abate-Shen, 2019). We took advantage of publicly available PCa transcriptomics and genomics studies to ascertain the alteration of *LKB1* in primary and metastatic lesions. We started by evaluating point mutations in a series of PCa datasets (Taylor et al., 2010, Cancer Genome Atlas Research Network, 2015; Kumar et al., 2016; Abida et al., 2017, 2019; Fraser et al., 2017; Armenia et al., 2018; Gerhauser et al., 2018) using cBioPortal (Cerami et al., 2012; Gao et al., 2013). The results revealed a lack of this type of alteration in PCa compared with a compendium of datasets from lung adenocarcinoma (Cancer Genome Atlas Research Network, 2013; Imielinski et al., 2012; Jordan et al., 2017), a tumor type with frequent alterations in *LKB1* (Fig. S1 G). We next focused on genomic aberrations using a large-scale study of PCa (n = 1,013), in which primary tumor biopsies and metastatic specimens where sequenced and tropism was annotated (Armenia et al., 2018). In this dataset, *LKB1* heterozygosity was observed in 24.6% of cases (249 out of 1,013), whereas complete loss was restricted to 3.36% of specimens (34 of 1,013; Table S2), in turn suggesting that LKB1 is not a commonly aberrant tumor suppressor in the prostate. However, we noted that metastatic tumors had higher rates of *LKB1* genomic aberrations, with 4.8% of homozygous deletions (16 of 333) compared with 2.65% in primary tumors (18 of 680), and 29.1% of heterozygous loss (97 of 333) compared with 22.35% in primary tumors (152 of 680; χ^2 P = 0.007). We decided to analyze whether perturbations in this gene could be associated with any specific metastatic behavior. 66% of metastatic cases presented site annotation (220 of 333). Metastatic cases within this subset with one or two intact alleles of *LKB1* exhibited similar distribution of metastasis, with a predominance of bone and lymph node dissemination and negligible lung metastasis (Fig. 1 G and Table S3). Among the limited number of metastatic cases with homozygous deletion of *LKB1*, 50% belonged to lung metastatic specimens (2 of 4; Fig. 1 G). The incidence of *LKB1* homozygous deletion was 28.6% (2 of 7, Fisher's exact test P < 0.01) in lung metastasis compared with 0.9% (2 of 213) of all other metastatic specimens, whereas we found no enrichment in bone metastasis or lymph node dissemination (Fig. 1 H, Fig. S1 H, and Table S3).

As a complementary approach, we analyzed an independent cohort (Kumar et al., 2016) in which we compared the expression of *LKB1* in the two predominant metastatic sites of interest, bone versus lung. In agreement with our previous results, lung metastatic lesions exhibited a significant reduction in the expression of the kinase (Fig. 1 I).

Taking advantage of the aforementioned large genomic dataset (Armenia et al., 2018), we explored the genetic events that could co-occur with *LKB1* in metastatic specimens. To this end, we extracted from this dataset the most frequent copy number alterations (Table S4) and evaluated their association to *LKB1* deletion in metastasis. We noted that none of the classic PCa oncogenic mutations were cooccurring with *LKB1* deletion

Downloaded from http://rupress.org/jem/article-pdf/217/6/e20191787/1780008/jem_20191787.pdf by guest on 09 February 2026

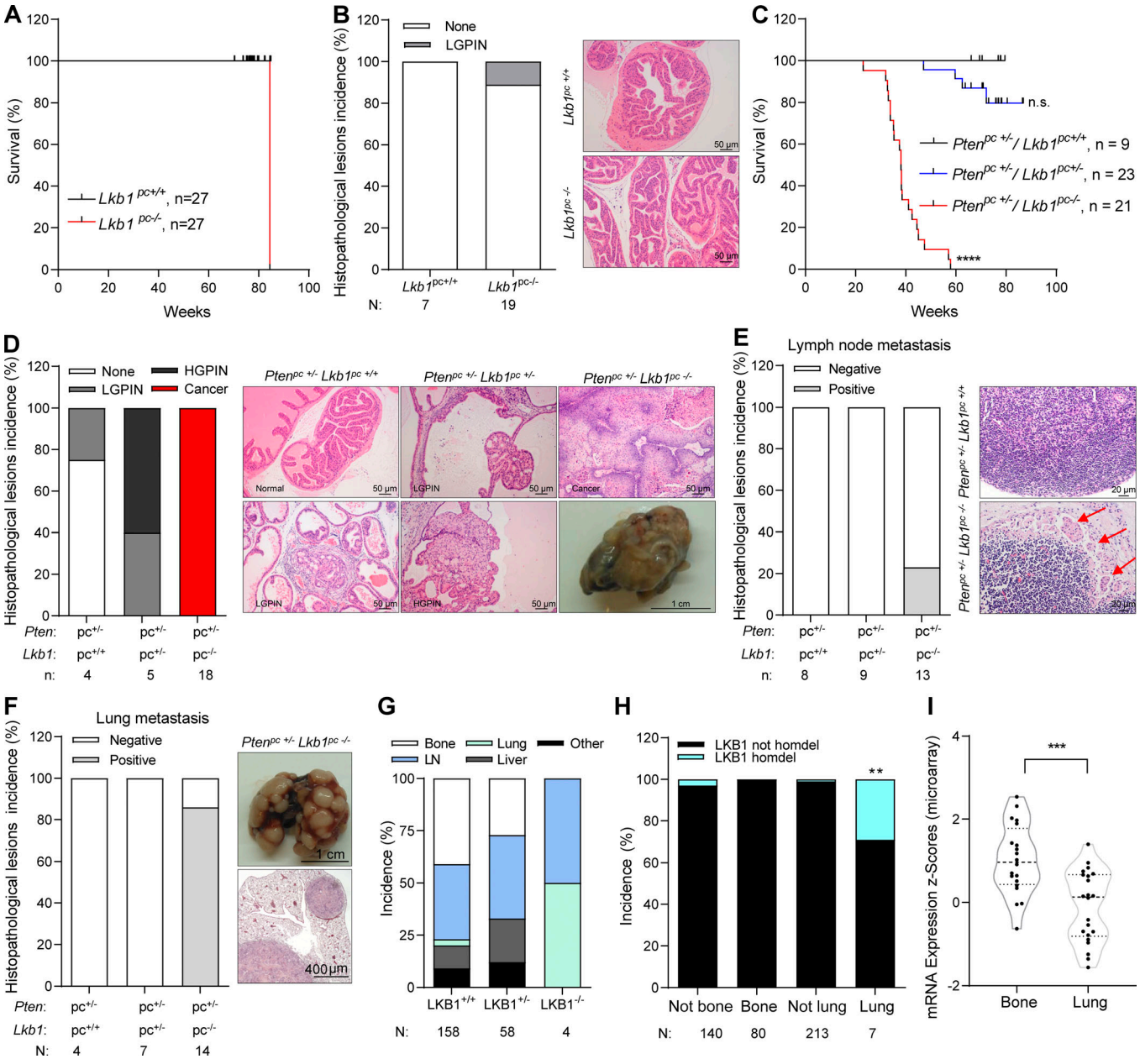

Figure 1. **Combined *Lkb1* loss with *Pten* heterozygosity in murine prostate epithelia results in PCa progression and dissemination. (A)** Cumulative survival curve (Kaplan–Meier survival plot) of $Lkb1^{pc+/+}$ (n = 27) and $Lkb1^{pc-/-}$ (n = 27) mice. The cumulative survival rate was plotted against age in weeks. **(B)** Histopathological characterization of the prostate in the indicated genotypes $Lkb1^{pc+/+}$ (n = 7) and $Lkb1^{pc-/-}$ (n = 19) mice (left). LGPIN, low-grade PIN. Representative image of H&E staining of normal prostate in $Lkb1^{pc+/+}$ mice (right, upper panel) and $Lkb1^{pc-/-}$ mice (right, lower panel). **(C)** Cumulative survival curve (Kaplan–Meier survival plot) of $Pten^{pc+/-}$ $Lkb1^{pc+/+}$ (n = 9), $Pten^{pc+/-}$ $Lkb1^{pc+/-}$ (n = 23), and $Pten^{pc+/-}$ $Lkb1^{pc-/-}$ (n = 21) mice. The cumulative survival rate was plotted against age in weeks. **(D)** Histopathological characterization of the prostate in the indicated genotypes: $Pten^{pc+/-}$ $Lkb1^{pc+/+}$ (n = 4), $Pten^{pc+/-}$ $Lkb1^{pc+/-}$ (n = 5), and $Pten^{pc+/-}$ $Lkb1^{pc-/-}$ (n = 18) mice (left). Right panels depict representative H&E micrographs of the histological features observed in each genotype. A macroscopic image of a representative tumor in $Pten^{pc+/-}$ $Lkb1^{pc-/-}$ mice is included. HGPIN, high-grade PIN. **(E)** Quantification of the frequency of lymph node colonization in $Pten^{pc+/-}$ $Lkb1^{pc+/+}$ (n = 8), $Pten^{pc+/-}$ $Lkb1^{pc+/-}$ (n = 9), and $Pten^{pc+/-}$ $Lkb1^{pc-/-}$ (n = 13) mice (left). Representative image of H&E staining of a normal lymph node in $Pten^{pc+/-}$ $Lkb1^{pc+/+}$ (right, upper panel) and a lymph node metastasis in $Pten^{pc+/-}$ $Lkb1^{pc-/-}$ mice (right, lower panel). Red arrows depict colonizing prostate tumor cells. **(F)** Quantification of the frequency of metastatic lesions in lung of $Pten^{pc+/-}$ $Lkb1^{pc+/+}$ (n = 4), $Pten^{pc+/-}$ $Lkb1^{pc+/-}$ (n = 7), and $Pten^{pc+/-}$ $Lkb1^{pc-/-}$ (n = 14) mice (left). Representative macroscopic image (right, upper panel) and representative histopathological image (right, lower panel) of metastatic lesions in lung in $Pten^{pc+/-}$ $Lkb1^{pc-/-}$ mice. **(G)** Incidence of metastatic lesions in bone, lymph nodes, lung, liver, and other tissues in patients with metastatic PCa with indicated *LKB1* genomic status. Numbers below the graph indicate total number of analyzed metastatic samples. Dataset of origin: Armenia et al. (2018). **(H)** Incidence of *LKB1* genomic alterations in metastatic specimens of patients with metastatic PCa (Armenia et al., 2018). Cases without *LKB1* homozygous deletion (*LKB1* not homdel); cases with *LKB1* homozygous deletion (homdel). Not bone, metastasis identified in all analyzed tissues except for bone; not lung, metastasis identified in all analyzed tissues except for lung. Numbers below the graph indicate total number of analyzed metastatic samples. **(I)** Gene expression levels of *LKB1* in bone and lung metastatic samples in patients with PCa (Kumar et al., 2016). pc, prostate-specific allelic changes; +, WT allele; –, deleted allele; n.s., not significant; **, $P < 0.01$; ***, $P < 0.001$. Statistic tests: log-rank (Mantel–Cox) test (A and C), Fisher exact test (H), two-tailed unpaired Student's t test (I).

Downloaded from http://rupress.org/jem/article-pdf/217/6/e20191787/1780008/jem_20191787.pdf by guest on 09 February 2026

(Table S5). These data led us to speculate that the aggressive features enabled upon *LKB1* loss are not associated with a single oncogenic hit, but rather to the process of transformation itself. In this regard, we envision the perturbation in *Pten* used in the mouse model as an illustrative oncogenic signal that would unleash prostate cell proliferation and enable the emergence of *Lkb1* loss–dependent phenotypes.

LKB1 phosphorylates 13 different effector kinases (Lizcano et al., 2004). To ascertain which of the potential targets of LKB1 could account for its prostate tumor–suppressive activity, we asked whether any of these targets would phenocopy the pattern of genomic loss of the master regulator using the same patient dataset (Armenia et al., 2018). When looking at the loci of the aforementioned kinases, we found genomic aberrations in only nine of them. Among these genes, we identified the strongest pattern of lung dissemination in *SIK3* (Fig. S1 I). Similar to *LKB1*, *SIK3* homozygous deletion was present in 28.6% (2 of 7, Fisher's exact test $P < 0.01$) of all lung metastatic cases (Fig. S1 J and Table S6). Interestingly, accounting for metastatic specimens with homozygous deletion in LKB1 and/or SIK3 increased the incidence in lung metastasis in this group to nearly 50% (3 of 7; Fisher's exact test $P < 0.01$; Fig. S1 K and Table S7). It is worth noting that the low number of specimens with alterations in these genes precluded a more conclusive result. The potential involvement of SIK3 in the prostate tumor–suppressive activity of LKB1 is coherent with recent reports in non–small cell lung cancer (Hollstein et al., 2019; Murray et al., 2019), in turn suggesting that the LKB1-SIK tumor suppressive axis might be relevant in different cancer types.

The aggressive nature of PCa in PTLK mice prompted us to characterize the molecular and pathological features of these tumors. PTLK prostate tissues exhibited reduced AMPK phosphorylation and elevated activity of mTOR complex 1 (by means of ribosomal protein S6 phosphorylation), in line with the reported inhibitory activity of LKB1 on this pathway (Momcilovic and Shackelford, 2015; Fig. S2, A and B). The histological analysis of PTLK lesions revealed that these tumors presented squamous features, with elevated p63 positivity and *Krt5* expression, in line with observations in other tumor types (Momcilovic and Shackelford, 2015; Fig. S2, B and C). We then compared the molecular features in PCa with intact *Lkb1* ($Pten^{pc-/-}$, PIN or adenocarcinoma as indicated) or *Lkb1* complete deletion (PTLK mice, squamous cell carcinoma). PIN lesions retained a well-defined layer of basal prostate cells, characterized by cytokeratin 5/6 (CK5/6) and p63, which were lost in invasive lesions (Fig. 2 A), in line with the notion that these tumors emerge from the aberrant proliferation of luminal cells (Arriaga and Abate-Shen, 2019). In contrast, prostate tumors and metastases in PTLK mice were predominantly composed of CK5/6- and p63-positive basal prostate cells and exhibited transcriptional signatures of squamous cell carcinoma in prostate tumor microdissected specimens (Fig. 2 A, Fig. S2 D, and Table S8). In agreement, prostate squamous cell carcinoma lesions from PTLK mice exhibited a 10-fold increase in basal cell proliferation, shown by Ki67, compared with adenocarcinoma lesions (Fig. S2 E). Our results support the notion that PCa in PTLK mice develops predominantly from the aberrant proliferation of basal cells, leading to highly metastatic squamous cell carcinoma.

The vast majority of available PCa high-throughput molecular studies focus on adenocarcinoma lesions, since this histological cancer type is predominant. However, according to PCa guidelines, squamous cell carcinoma of prostate presents an incidence of 0.5–1% and exhibits highly aggressive characteristics (Brunnhoelzl and Wang, 2018; Munoz et al., 2007). We searched for *LKB1*-deficient PCa specimens that exhibited squamous pathological features. Interestingly, we identified three such cases (Fig. 2 B). Two of the three cases exhibited positivity for 34βE12, a basal cell marker, whereas one case showed weak positivity. Interestingly, two of these three specimens harbored combined *LKB1* and *PTEN* alterations, analogous to our murine model (Fig. 2 B).

To approach the mechanism by which LKB1 suppresses PCa, we characterized a panel of PCa cells. In line with previous reports, DU145 cells lack LKB1 protein expression, due to a frameshift homozygous mutation (Ikediobi et al., 2006; Fig. 3 A). We took advantage of this cell line and reintroduced *LKB1* at expression levels comparable to other prostate cells. As a technical control, we also reexpressed a reported kinase activity-defective mutant, $LKB1^{K78I}$ (Fig. 3 B and Fig. S2 F; Shaw et al., 2004). Whereas reintroduction of LKB1 did not affect two-dimensional cell growth (Fig. S2 G), we observed a remarkable inhibition of migration, invasion, invasive growth, and anchorage-independent growth in both WT and K78I mutant LKB1-expressing cells (Fig. 3, C–E; and Fig. S2 H). We extended our studies to xenograft assays. At the level of both subcutaneous tumor growth and metastatic dissemination, LKB1 was tumor suppressive regardless of its kinase activity (Fig. 3, F–I; and Fig. S2, I and J).

The results with $LKB1^{K78I}$ were suggestive of an unprecedented kinase-independent tumor-suppressive activity. We ruled out this possibility by different means. On the one hand, we evaluated the correct and equivalent formation of the LKB1 complex in cells (Boudeau et al., 2003; Momcilovic and Shackelford, 2015). By both coimmunoprecipitation coupled to Western blot and mass spectrometry analysis, we could demonstrate that $LKB1^{WT}$ and $LKB1^{K78I}$ presented equivalent protein interaction profiles with core components of its functional complex, including MO25, STE20-related adaptor, HSP90 and CDC37 (Fig. S3, A and B; and Table S9). On the other hand, the kinase-independent effect could be due to the sequestration of MO25 away from other STK family proteins. *MO25A* was the predominant isoform in these cells (Fig. S3 C). We hypothesized that, if the tumor suppressive activity of both LKB1 constructs relied on the sequestration of MO25, silencing this gene would mimic LKB1 expression and elicit tumor suppression. However, the silencing of this adaptor protein did not reduce two-dimensional or anchorage-independent growth (Fig. S3, D–F).

The lack of evidence supporting a kinase-independent tumor suppressive function of LKB1 prompted us to carefully monitor the impact of K78I mutation on the activity of the kinase. Surprisingly, $LKB1^{K78I}$ retained 10% of the WT activity (Fig. 4 A). We evaluated the impact of LKB1 expression on the activity of its targets. In line with our clinical observations, the phosphorylation of SIK1-3 was increased by $LKB1^{WT}$ and to a lower extent by the K78I mutant (Fig. 4 B), and this effect was retained, albeit with lower amplitude, when monitoring AMPK activity (Fig. S3, G and H). To ascertain whether the residual activity of $LKB1^{K78I}$

Downloaded from http://rupress.org/jem/article-pdf/217/6/e20191787/1780008/jem_20191787.pdf by guest on 09 February 2026

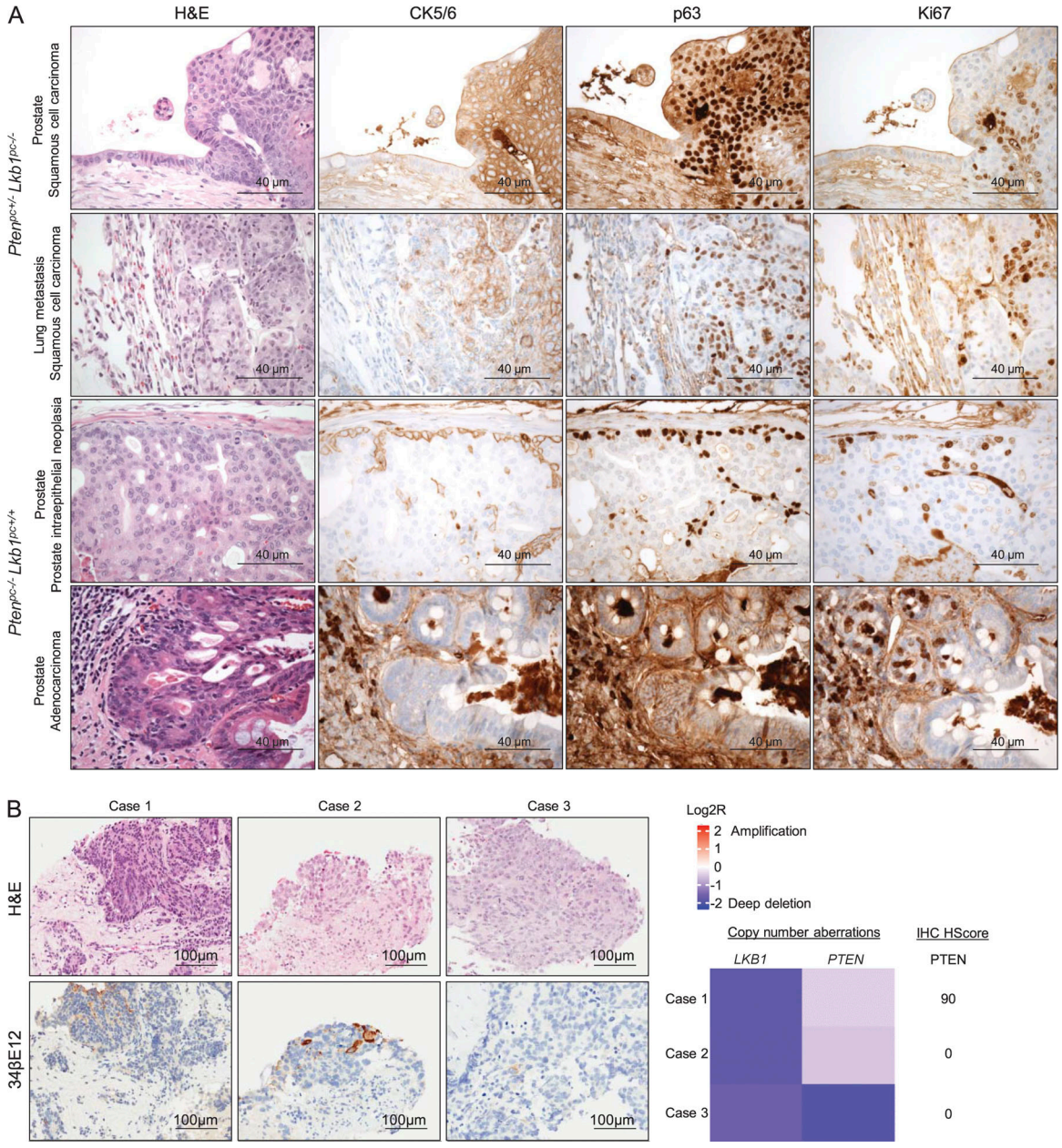

Figure 2. **Histological characterization of prostate tumors with *LKB1* deficiency. (A)** Immunostaining images of H&E, CK5/6, p63, and Ki67 in squamous cell carcinoma of prostate (*Pten*$^{pc+/-}$ *Lkb1*$^{pc-/-}$ mice), lung metastasis (*Pten*$^{pc+/-}$ *Lkb1*$^{pc-/-}$ mice), PIN lesions (*Pten*$^{pc-/-}$ *Lkb1*$^{p+/+}$ mice), and adenocarcinoma (*Pten*$^{pc-/-}$ *Lkb1*$^{p+/+}$ mice). **(B)** Immunohistochemical images of H&E (left, upper panels) and 34βE12 (left, lower panels) in PCa specimens with squamous features. Right panels depict the status of *LKB1* (genomic) and *PTEN* (genomic and protein).

is sufficient to exert tumor suppression, we generated a second mutant, harboring a nucleotidic change in the magnesium-binding domain (D194A; Lizcano et al., 2004) that we confirmed to be fully devoid of kinase activity (Fig. 4 C and Fig. S3 I). Importantly, compared with the deleted parental cells, the expression of LKB1^{D194A} neither activated SIK1-3 nor influenced the signaling pattern or the biological response in vitro and in vivo, as opposed to LKB1^{WT} or LKB1^{K78I} mutant (Fig. 4, D–G; and Fig. S3, J–O). Altogether, our results demonstrate that loss of LKB1 is associated with the emergence of squamous features in murine PCa and that the kinase requires minimal activity to suppress aggressive PCa features in cellular systems.

PCa is a highly prevalent disease in men. Although it is generally considered curable with first-line therapies, a fraction of patients will exhibit biochemical recurrence associated with the failure on subsequent therapeutic alternatives (Chang et al., 2014). These men will eventually develop metastatic disease, thus accounting for the mortality of the disease, together with those individuals that exhibit metastatic PCa at presentation (James et al., 2015). Bone is the predominant site of metastasis in this disease, although a subset of highly aggressive PCa disseminates to the lung and soft tissues (Arriaga and Abate-Shen, 2019). The biology of lethal metastatic PCa is poorly understood, and there are few murine models to date that recapitulate this

Downloaded from http://rupress.org/jem/article-pdf/217/6/e20191787/1780008/jem_20191787.pdf by guest on 09 February 2026

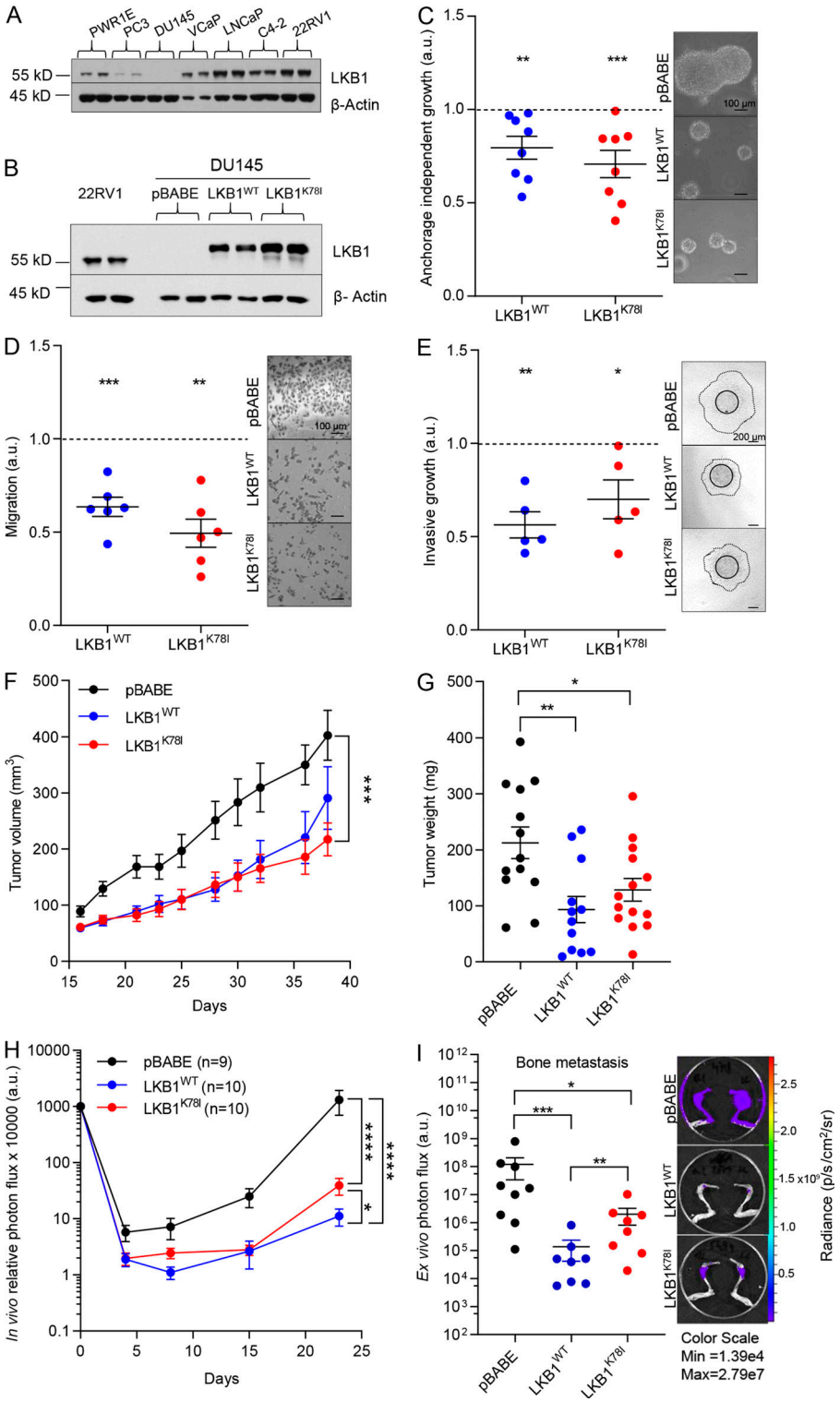

Figure 3. **WT and mutant LKB1^{K78I} exert significant tumor suppressive activity. (A)** Western blot analysis of LKB1 protein expression in a normal prostate epithelial cell line (PWR1E) and in a panel of PCa cell lines (technical duplicates are shown). Representative image from three independent experiments is shown. **(B)** Western blot analysis of LKB1 protein expression in DU145 cell line with ectopic expression of WT Flag-LKB1 (LKB1^{WT}), the Flag-LKB1-K78I mutant (LKB1^{K78I}), or transduced with mock vector (pBABE) using 22RV1 cells as a positive control (n = 3). Representative image from three independent experiments is shown. **(C–E)** Quantification (left) and representative image (right) of anchorage-independent growth (C; n = 8, independent experiments), migration (D; n = 6, independent experiments), and invasive growth (E; n = 5, independent experiments). Black circle highlights the original size of the spheroid and dashed line highlights the size of the spheroid after 48 h of incubation in DU145 cells with ectopic expression of LKB1^{WT} or LKB1^{K78I} or transduced with mock (pBABE). Data are normalized to control (pBABE; dashed line). **(F and G)** Effect of LKB1 reconstitution in DU145 cells with ectopic expression of LKB1^{WT} or LKB1^{K78I} or transduced with mock (pBABE) on tumor formation (F) and tumor weight (G; left). n = 13–14 tumors per condition. **(H and I)** Evaluation of metastatic capacity of control (pBABE) and LKB1^{WT}- and LKB1^{K78I}-expressing DU145 cells using intracardiac xenotransplant assays. Luciferase-based signal intensity of DU145 cells in limbs was monitored in vivo (H; n as indicated) and ex vivo (I; mean signal of both tibia was calculated and presented; n as indicated in the dot plot) for ≤38 d. Representative luciferase images are presented referred to the quantification plots. Statistic tests: one-sample t test (C–E), one-tailed unpaired Student's t test (F and G), one-tailed Mann–Whitney U test (H and I). *, P < 0.05; **, P < 0.01; ***, P < 0.001; ****, P < 0.0001. Error bars represent SEM.

pattern of aggressiveness (Arriaga and Abate-Shen, 2019). Our study provides the field with an invaluable model to study the process of PCa dissemination in an immune-competent and tissue-specific context. Importantly, our patient dataset analysis using the largest cohort available (Armenia et al., 2018) shows that homozygous deletion in *LKB1* is rare in PCa (2.6% in primary tumors and 4.8% in metastasis), and point mutations are negligible. Despite this low frequency of *LKB1* homozygous deletion, we find an association of this event with metastasis in the lung. It is important to note that our data in murine models and human specimens is insufficient to postulate a role for LKB1 in metastatic tropism. However, together with the in vitro assays, our data indicate that LKB1 deletion results in the acquisition of aggressiveness features, which would enable prostate tumor cells to gain access to the lung instead of the long metastatic process that underlies bone colonization.

Downloaded from http://rupress.org/jem/article-pdf/217/6/e20191787/1780008/jem_20191787.pdf by guest on 09 February 2026

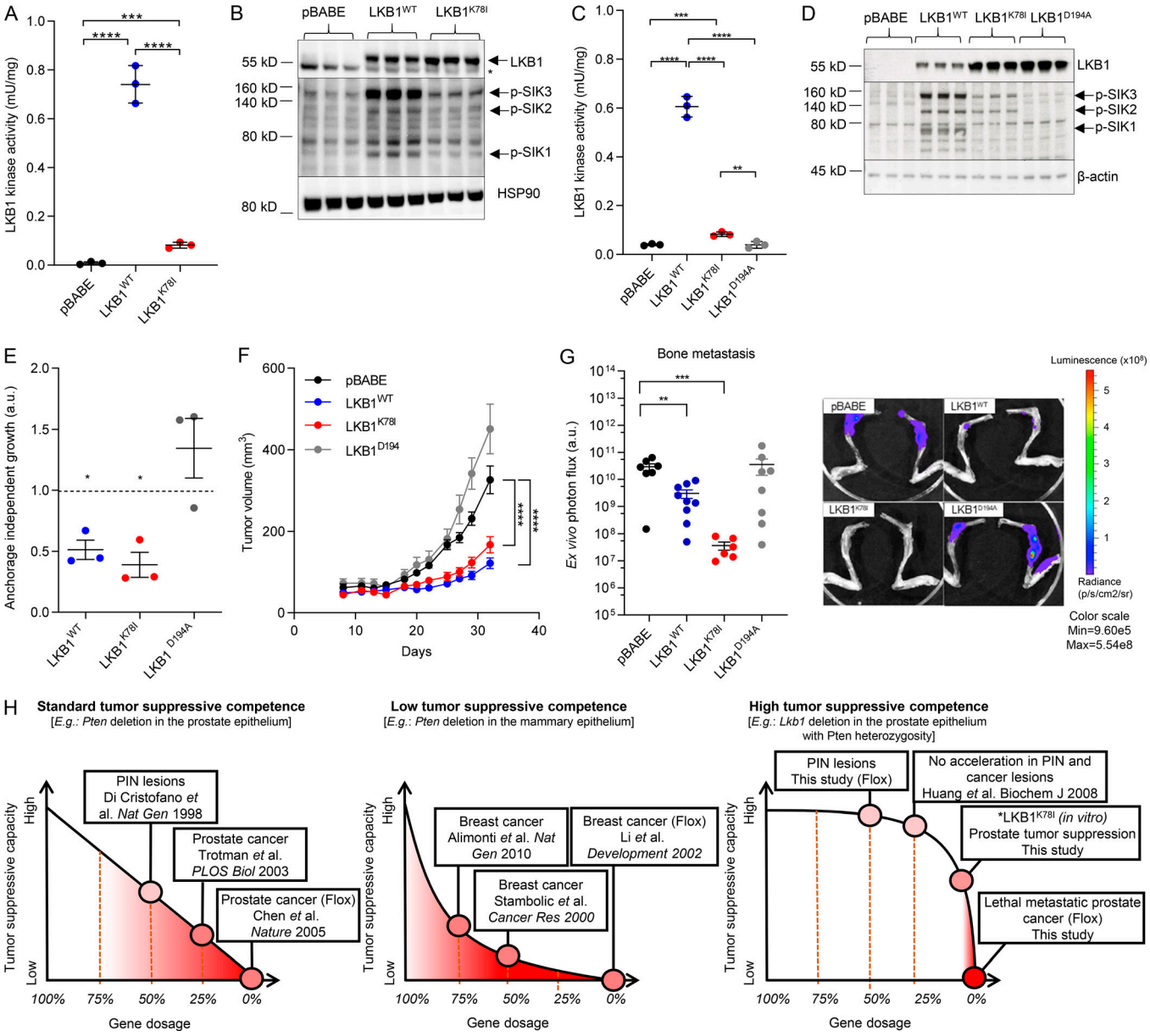

Figure 4. **LKB1 is a high-competence prostate tumor suppressor. (A)** Evaluation of LKB1 kinase activity of DU145 cell line with ectopic expression of LKB1^{WT} or LKB1^{K78I} or transduced with mock (pBABE). Representative data from three independent experiments. **(B)** Western blot analysis for LKB1, SIK1-3 phosphorylation, and HSP90 protein expression in control and LKB1^{WT}- and LKB1^{K78I}-expressing cells. The asterisk indicates a nonspecific band. Representative image from three independent experiments is shown. **(C)** Evaluation of LKB1 kinase activity of DU145 cell line with ectopic expression of LKB1^{WT}, LKB1^{K78I}, or LKB1^{D194A} or transduced with mock (pBABE). Representative data from two independent experiments. **(D)** Western blot analysis for LKB1, SIK1-3 phosphorylation, and β-actin protein expression in control, LKB1^{WT}-, LKB1^{K78I}-, and LKB1^{D194A}-expressing cells. Representative image from three independent experiments is shown. **(E)** Effect of LKB1^{WT}, LKB1^{K78I}, and LKB1^{D194A} expression on anchorage-independent growth (n = 3, independent experiments). Data are normalized to control (pBABE; dashed line). **(F)** Effect of LKB1 reconstitution in DU145 cells with ectopic expression LKB1^{WT}, the kinase-defective mutants (LKB1^{K78I}, LKB1^{D194A}) or infected with mock vector (pBABE) on tumor formation in xenotransplantation experiments (n = 20 injections per condition). **(G)** Metastatic capacity of control (pBABE), LKB1^{WT}-, LKB1^{K78I}-, and LKB1^{D194A}-expressing DU145 cells using intracardiac xenotransplant assays. Quantification (left) and representative tibia view (right) of luciferase-dependent signal intensity of DU145 cells in ex vivo tibia analysis on day 42 after injection (mean signal of both tibias was calculated and presented; n as indicated in the dot plot). **(H)** Schematic representation of the proposed classification of tumor suppressors according to their competence. Flox, results based on tissue-specific conditional mouse models. Red filling, oncogenic features associated to dose reduction. Statistic tests: one-tailed unpaired Student's t test (A, C, and F); one-sample t test (E), one-tailed Mann–Whitney U test (G). n.s., not significant; *, P < 0.05; **, P < 0.01; ***, P < 0.001; ****, P < 0.0001.

Lkb1 deletion is associated with the onset of metastatic disease in other tumor types when combined with perturbation of different cancer genes (Momcilovic and Shackelford, 2015). Overall, experimental evidence suggests that loss of *LKB1* is not an initiating event in cancer, but rather an enhancer of aggressive features once oncogenic signaling is present. Following this line of reasoning, and in line with our patient analysis, it is tempting to speculate that the oncogenic signaling provides a proliferative advantage to cells, regardless of the cancer gene perturbed, that will unleash the metastasis-suppressor potential of LKB1.

Downloaded from http://rupress.org/jem/article-pdf/217/6/e20191787/1780008/jem_20191787.pdf by guest on 09 February 2026

Squamous cell carcinoma is included in the clinical guidelines as a highly aggressive subtype of PCa, with an incidence of 0.5–1% and average survival of 14 mo after diagnosis (Brunnhoelzl and Wang, 2018; Munoz et al., 2007). The combination of *Pten* and *Lkb1* deletion in the prostate epithelium performed in this study results in aggressive squamous cell prostate carcinoma. In line with the notion that basal prostate cells have reduced androgen requirements (Xie et al., 2017), PTLK tumors exhibit delocalized or negative AR expression. It is worth highlighting the different cellular compartments that contribute to PCa aggressiveness upon loss of tumor suppressors. *Lkb1* loss affects basal cell proliferation. In contrast, deletion in other tumor suppressors such as Tp53 predominantly favors luminal cell renewal and expansion (Agarwal et al., 2015). Importantly, whereas the incidence is low in human PCa, mouse models of PCa are more prone to exhibit squamous features (Ittmann et al., 2013; Martin et al., 2011). In addition, several studies report that *Lkb1* deletion in different tissues predisposes to squamous lesions (Momcilovic and Shackelford, 2015). Specifically, combined deletion of *Pten* and *Lkb1* in the lung was recently reported as the first bona fide mouse model of lung squamous cell carcinoma (Xu et al., 2014). Interestingly, the existence of compound *LKB1* and *PTEN* deletions in human prostate tumors with squamous pathological and molecular features opens an avenue of research toward better understanding of this disease.

The introduction of hypomorphic alleles in mouse models has enabled the fine-tuning of dosage beyond the use of gene knockouts. Taking advantage of this technology, we previously reported that *Pten* is a weak breast tumor suppressor, since the introduction of a hypomorphic allele in heterozygosity (70–75% of WT *Pten* expression) resulted in breast cancer (Alimonti et al., 2010). The combined use of conditional mouse models and LKB1 mutant in cells in this study provides strong support for the notion that this kinase is a potent prostate tumor suppressor that can operate at very low doses. Moreover, our analysis of the mutant $LKB1^{K78I}$ provides a feasible explanation for the discordance of our results with the elegant study performed by Huang et al. (2008). Using a whole-body hypomorphic *Lkb1* mutant mouse combined with systemic *Pten* heterozygous deletion, they observed that there was *Lkb1* dose-dependent acceleration of various cancerous lesions. However, $Pten^{+/-};Lkb1^{Hy/Hy}$ mice did not exhibit alterations in prostate pathology compared with $Pten^{+/-};Lkb1^{+/+}$. Our report, together with past results from our group and others, suggests that classic genetic dosage distributions or definitions such as haploinsufficiency are unable to correctly define the extent of their role in cancer.

We put forward the concept of tumor suppressive "competence" as a defining feature of tumor suppressors, taking *PTEN* and *LKB1* as illustrative genes (Fig. 4 H). We define standard competence as a continuum of reduction in tumor suppression capacity along with the dosage, which is recapitulated in the prostate phenotype of *Pten* mutant mice (Nardella et al., 2010; Chen et al., 2005; Di Cristofano et al., 1998; Trotman et al., 2003). We define low competence as a reduction of <50% when a tumor suppressor gene dose results in cancerous lesions, as reported in the mammary tissue with *Pten* mutants expressing 75% of *Pten* (Alimonti et al., 2010) and at lower gene doses by others (Stambolic et al., 2000; Li et al., 2002). The integration of our results with the study of the group of Alessi (Huang et al., 2008) justifies the definition of LKB1 as a prostate tumor suppressor with high competence. In this context, reduction of the gene dosage of 50% (heterozygous) or 70% (hypomorphic) is inconsequential for PCa development. Moreover, retention of LKB1 activity as low as 10% is sufficient for the kinase to exert tumor suppression in vitro and in vivo. Only complete deletion of this gene is associated with the pathogenesis of PCa, a genetic condition that turns a premalignant disease (PIN, typical of $Pten^{+/-}$ mice) into lethal metastatic PCa. It is worth noting that the introduction of competence in the definition of tumor suppressors remains a conceptual implementation, based on the integration of results derived from conditional and germline mouse models of two exemplifying genes, *PTEN* and *LKB1*. Further research is warranted to explore the relevance of this concept for other tumor suppressors, but it could harbor therapeutic relevance, since it would help establish the extent of pathway reactivation required for targeted therapies to show clinical effectiveness.

Materials and methods

Genetically engineered mouse models

The conditional tissue-specific phosphatase and tensin homologue (Pten) knockout (C57/BL6/129sv; Pb-Cre4; Pten lox/lox) model was kindly provided by Pier Paolo Pandolfi (Beth Israel Deaconess Cancer Center, Boston, MA). The conditional tissue-specific Lkb1 null homogeneous background model (FVB;Lkb1lox/lox) was from Mouse Models of Human Cancer Consortium in a pure FVB background. First, we backcrossed this line into *C57BL*/6J for four generations to obtain animals with genetic background enriched in C57/BL6 (>90% C57/BL6). Next we crossed Lkb1lox/lox mice with Pb-cre4 and Pten lox/lox mice for at least four generations to obtain a founder colony with mixed homogeneous background, and experimental animals were generated. Littermates where analyzed when possible. However, due to the complexity of the allele combination, the different genotypes of interest with *Pten* and/or *Lkb1* alteration were obtained from parallel contemporary breeding pairs. Probasin Cre was always retained in male mice, since in females Pb-Cre4 expression in utero can lead to recombination in embryos during pregnancy. The Cre recombinase expression, under the control of androgen-dependent ARR2B probasin promoter (Pb-Cre4), allowed the deletion of Pten in the prostate epithelium at puberty. Prostate Pten/Lkb1-deleted male mice were termed $pc^{-/+}$ (heterozygous) or $pc^{-/-}$ (homozygous knockout) for each gene.

Patient cohort and ethics approval

Patients were identified from a cohort of men with advanced castrate-resistant PCa treated at the Royal Marsden National Health Service Foundation Trust. All patients had given written informed consent and were enrolled in institutional protocols approved by the Royal Marsden Hospital (London, UK) ethics review committee (reference no. 04/Q0801/60).

Generation of stable cell lines

DU145 cells expressing WT LKB1 ($LKB1^{WT}$), LKB1 K78I ($LKB1^{K78I}$), and LKB1 D194A ($LKB1^{D194A}$) mutants were generated by retroviral

Downloaded from http://rupress.org/jem/article-pdf/217/6/e20191787/1780008/jem_20191787.pdf by guest on 09 February 2026

gene transfer. pBABE-puro (Addgene plasmid 1764; RRID:Addgene_1764) was a gift from Hartmut Land (Imperial Cancer Research Fund, Lincoln's Inn Fields, London, UK), Jay Morgenstern, and Bob Weinberg (Whitehead Institute for Biomedical Research, Cambridge, MA; Morgenstern and Land, 1990). pBABE-FLAG-LKB1 (Addgene plasmid 8592; RRID:Addgene_8592) and pBABE-FLAG-KD LKB1 (Addgene plasmid 8593; RRID:Addgene_8593) were a gift from Lewis Cantley (Meyer Cancer Center, New York, NY; Shaw et al., 2004). pBabe-FLAG-LKB1-D194A was a gift from Dr. Bin Zheng (Columbia University, New York, NY).

Lentiviral shRNA constructs targeting MO25α (TRCN0000044254; TRCN0000044256) were purchased from Sigma-Aldrich, and a scramble shRNA (hairpin sequence: 5′-CCGGCAACAAGATGAAGAGCACCAACTCGAGTTGGTGCTCTTCATCTTGTTG-3′) was used as control. pLKO.1 puro was a gift from Bob Weinberg (Addgene plasmid 8453; RRID:Addgene_8453; Stewart et al., 2003).

HEK293FT cells were transfected with retroviral or lentiviral vectors following standard procedures, and viral supernatant was used to infect cells. Selection was done using puromycin (2 µg/ml; Sigma-Aldrich).

Cell culture

Human prostate carcinoma cell lines PC3, DU145, and LNCaP were purchased from Leibniz-Institut Deutsche Sammlung von Mikroorganismen und Zellkulturen GmbH, who provided an authentication certificate. Human prostate cell line PWR1E and human prostate carcinoma cell lines 22RV1 and VCaP were purchased from ATCC. HEK293FT and C4-2 were generously provided by the laboratories of Rosa Barrio (CIC bioGUNE, Derio, Spain) and Pier Paolo Pandolfi, respectively. Cell lines were periodically subjected to microsatellite-based identity validation. The cell lines used in this study were not found in the database of commonly misidentified cell lines maintained by the International Cell Line Authentication Committee and National Center for Biotechnology Information Biosample. All cell lines were routinely monitored for mycoplasma contamination and quarantined while treated if positive. DU145, PC3, VCaP, and 293FT cell lines were maintained in DMEM supplemented with 10% (vol/vol) FBS (Gibco) and 1% (vol/vol) penicillin-streptomycin (Gibco). LNCap, C4-2, and 22RV1 cell lines were maintained in RPMI supplemented with 10% (vol/vol) FBS and 1% (vol/vol) penicillin-streptomycin. PWR1E cell line was maintained in Keratinocyte Serum Free Medium (Gibco) supplemented with 0.05 mg/ml bovine pituitary extract (Gibco) and 5 ng/ml epidermal growth factor (Gibco).

Cellular assays

Cell proliferation

1×10^4 cells were plated in triplicate in 12-well dishes. Quantification was performed as reported (Torrano et al., 2016). Anchorage-independent growth was tested by the ability to grow in soft agar as described previously (Torrano et al., 2016). The cell migration and invasion assay was performed in a 24-well-size Transwell plate of 8-µm pores (BD Falcon 351185). The invasive growth assay was performed as referenced (Martín-Martín et al., 2018) using the hanging drop method.

Anchorage-independent growth

A 6-well tissue culture dish was coated with the bottom agar layer (complete DMEM containing 0.6% agar; SeaKem LE agarose, Lonza) and stored at 4°C for ≥30 min to let the agar solidify. Cells (2,500 cells/well) were resuspended in a 0.3% low-melting-point agar (Agarose LM, Pronadisa, Conda) and plated on top of the bottom agar. The plates were incubated (37°C and 5% CO_2) for 4 wk for growth of colonies. Colonies were counted using Fiji software.

Cell migration assay

Cells (50,000 cells/well) were resuspended in final volume of 500 µl 0.1% FBS DMEM and seeded in the upper part of the chamber. The bottom part was filled with 1.4 ml of complete DMEM. Plates were maintained at 37°C and 5% CO_2 for 24 h. Nonmigrated cells from the upper surface of the membrane were carefully removed by rinsing with PBS and using a cotton swab. The membrane was fixed with 10% formalin (15 min at 4°C) and stained with crystal violet. Transwell invasion was performed using Matrigel-coated chambers (Corning BioCoat Matrigel Invasion Chamber). After an incubation period of 48 h (37°C and 5% CO_2), membrane washing and fixation were performed under the same conditions as in the migration assay. Both Transwell assays were evaluated by photomicrographs from five randomly chosen fields (100×) per membrane. The number of migrated or invaded cells was counted using Fiji.

Invasive growth assay

28,000 cells were resuspended in a final volume of 500 µl DMEM with 6% methylcellulose (Sigma-Aldrich, M0387). Drops (25 µl/drop) were pipetted on the cover of a 100-mm culture plate. The inverted plates were incubated at 37°C and 5% CO_2 for 48 h. Once formed, spheroids were collected, resuspended in collagen I solution (1.7 mg/ml in DMEM), and seeded into 24-well plates that were maintained at 37°C and 5% CO_2 for 48 h. The area of the invading spheroids was measured using Fiji. Relative invasive growth was quantified as area difference on day 2 minus day 0.

Xenotransplant assays

All mouse experiments were performed following the ethical guidelines established by the Biosafety and Welfare Committee at the Center for Cooperative Research in Biosciences as previously described (Martín-Martín et al., 2018; Torrano et al., 2016). The procedures employed were performed following the recommendations from Association for Assessment and Accreditation of Laboratory Animal Care. DU145 cells (pBABE, $LKB1^{WT}$, $LKB1^{K78I}$, and $LKB1^{D194A}$; 4×10^6 cells per site) were resuspended in a final volume of 100 µl cold PBS supplemented with glucose (5 µM) mixed with 50 µl of Matrigel (Corning) and injected subcutaneously in two flanks per 6–12-wk-old male athymic nude mouse. Measurement of tumor size was performed three times a week, and tumor volume was estimated using the following formula: volume = length × width^2 × 0.526. After euthanasia, tumors were weighed, and tissue was fresh frozen or fixed overnight in 10% neutral buffered formalin, embedded in paraffin, sectioned 3-µm thick, and dried. Proliferation was assessed in

Downloaded from http://rupress.org/jem/article-pdf/217/6/e20191787/1780008/jem_20191787.pdf by guest on 09 February 2026

dewaxed and rehydrated slides using Ki67 antibody (MA5-14520, Thermo Fisher Scientific).

Metastasis assays

All animal studies were performed according with the institutional animal care and use committee of Institute for Research in Biomedicine, Barcelona, Spain. For these studies, male BALB/c nude mice (Harlan) were used (12 wk old). Before cell injection, mice were anaesthetized as previously described (Torrano et al., 2016). Using a 26-G needle, 500,000 cells were injected into the left cardiac ventricle of mice resuspended in 1× PBS. Luciferase activity from the bone legs was detected by IVIS imaging. Data were processed using Living Image software. Photon Flux was measured every week for 38–42 d and normalized to values obtained on day 0. Ex vivo tibia analysis was performed in those mice with evidence of bioluminescence signal above background and that survived for the entire experiment.

Histopathologic analysis, immunohistochemistry, and immunofluorescence

Tissue sample collection (prostate gland, lymph nodes, long bones from lower limbs, lungs, and liver) was performed at 18 mo of age ($LKB1^{pc+/+}$ and $LKB1^{pc-/-}$ mice) or 10 mo of age ($Pten^{pc+/-}$ $LKB1^{pc+/+}$, $Pten^{pc+/-}$ $LKB1^{pc+/-}$, and $Pten^{pc+/-}$ $LKB1^{pc-/-}$). Tissue samples were fixed overnight in 10% neutral buffered formalin, embedded in paraffin, sectioned 3-µm thick, and dried. Slides were dewaxed and rehydrated through a series of graded ethanol to water and stained with the required antibody and/or H&E.

Histological observations on H&E-stained tissues were performed using an Olympus DP73 digital camera. Prostatic lesions were histologically classified according to the criteria of the Consortium Prostate Pathology Committee (Shappell et al., 2004) and scored as 0, no lesion observed; 1, focal or multifocal low-grade PIN; 2, focal or multifocal high-grade PIN; 3, carcinoma affecting <50% of tissue; 4, carcinoma affecting >50% of tissue. SPCs originate from squamous metaplasia of neoplastic prostatic epithelial cells. Lungs metastasis were described as micrometastasis when neoplastic cell growth in a small focus or multifocal or severe metastasis when neoplastic cells progressed involving multiple or large lung regions. Lymph node lesions were scored as follows: 0, no lesion observed; or 1, metastasis.

A standard immunohistochemistry protocol was applied. Briefly, slides were deparaffinized, and antigen retrieval was performed in a pressure cooker in citric acid buffer, pH 6 (phospho-S6, p63) or EDTA, pH 8 (phospho-AMPK). Sections were then immersed in 3% hydrogen peroxide to block endogenous peroxidase activity and washed in PBS. Incubation with specific blocking serum for 30 min was followed by incubation with primary antibodies at 4°C overnight using the following concentrations: phospho-AMPK (CST, 2535, 1:50), phospho-S6 (CST, 4858, 1:500), p63 (Abcam, ab735, 1:100), and AR (Santa Cruz Biotechnology, N-20, 1:200). The next day, after washing in PBS, signal was amplified with avidin/biotin technology (Vectastain Elite ABC system) or ImmPress HRP IgG (Peroxidase) Polymer Detection Kit (Vector Laboratories) and visualized with ImmPact DABSubstrate (Vector Laboratories). Finally, tissues were counterstained with H&E.

CK5/6 (Ventana, 790-4554, ready to use, cytoplasmic staining), p63 (Ventana, 790-4509, ready to use, nuclear staining), and Ki67 (Ventana, 790-4286, ready to use, nuclear staining) stains were performed in automated immunostainers (BenchMark Ultra, Ventana Medical Systems) following routine methods. Tris-EDTA was used for antigen retrieval. Negative controls were slides not exposed to the primary antibody, and these were incubated in PBS and then processed under the same conditions as the test slides. The analysis was performed using a Nikon Eclipse 80i microscope.

High molecular weight CK immunohistochemistry was performed on the Bond RX automated platform (Leica Microsystems) using a mouse monoclonal anti–high molecular weight CK antibody (Abcam, ab776, clone 34βE12). Heat-induced epitope retrieval was achieved with Bond Epitope Retrieval Solution 2 (Leica Microsystems, AR9640) for 20 min at 100°C before incubation with primary antibody (1:100 dilution) for 15 min at room temperature. The reaction was visualized using the Bond Polymer Refine Detection system (DS9800, Leica Microsystems).

PTEN immunostaining and scoring criteria was done following the procedure in Ferraldeschi et al. (2015). Proliferative basal epithelium cells were identified by staining with Ki67 (Thermo Fisher Scientific, 1/200, 14-5698-82) and CK5 (BioLegend, 1/500, PRB-160P) primary antibodies. For quantification of double-positive cells, five independent sections from five independent mice were counted using ImageJ 1.52a (National Institutes of Health).

LKB1 kinase activity

LKB1 kinase activity was measured as described previously (Lizcano et al., 2004). Cells stably overexpressing LKB1 WT, K78I, or D194A mutants (FLAG-tagged), were used to immunoprecipitate anti-FLAG-agarose resin, in triplicate. Reactions were performed in FLAG-agarose immunoprecipitates from 1.5 mg protein, using 200 µM NuaKtide as peptide and 100 µM ^{32}P-ATP as substrates in a 60-min reaction. 1 mU of LKB1 kinase activity is the amount that catalyzed the phosphorylation of 1 pmol of NuaKtide in 1 min in the standard assay at 30°C.

Quantitative real-time PCR (qRT-PCR)

RNA was extracted using NucleoSpin RNA isolation kit (Macherey-Nagel, 740955.240C). For animal tissues, a Trizol-based implementation of the NucleoSpin RNA isolation kit protocol was used as reference (Ugalde-Olano et al., 2015). For all cases, 1 µg of total RNA was used for cDNA synthesis using Maxima H Minus cDNA Synthesis Master Mix (Thermo Fisher Scientific, M1682). qRT-PCR was performed as previously described (Carracedo et al., 2012). Universal Probe Library primers (Roche) and probes (Roche and Thermo Fisher Scientific) are detailed in Table S10. All qRT-PCR data presented were normalized using GAPDH/Gapdh (Applied Biosystems, Hs02758991_g1, Mm99999915_g1).

Western blot

Western blot was performed as previously described (Carracedo et al., 2012). Briefly, cells were lysed in radioimmunoprecipitation assay buffer (50 mM Tris-HCl, pH 7.5, 150 mM NaCl, 1 mM EDTA, 0.1% SDS, 1% Nonidet P40, 1% sodium deoxycholate, 1 mM sodium fluoride, 1 mM sodium orthovanadate, 1 mM β-glycerophosphate,

Downloaded from http://rupress.org/jem/article-pdf/217/6/e20191787/1780008/jem_20191787.pdf by guest on 09 February 2026

and protease inhibitor cocktail; Roche). Antibodies used were phospho-AMPK substrate motif (CST 5759), phospho-ACC (CST 11818), phospho-AMPK (CST 2535), LKB1 (CST 3050), MO25α/CAB39 (CST 2716s), PTEN (CST 9559), phospho-Raptor (CST 2083), Raptor (CST 2280), β-actin (CST 3700S), and HSP90 (CST 4874). All antibodies were used at a 1:1,000 dilution except β-actin at 1:2,000. Mouse and rabbit secondary antibodies were purchased from Jackson Immunoresearch. After standard SDS-PAGE and Western blotting techniques, proteins were visualized using the enhanced chemiluminescence.

Proteomics

Immunoprecipitation

Cells were lysed in immunoprecipitation buffer (40 mM Tris-HCl, pH 7.5, 1 mM EDTA, 150 mM NaCl, 0.5% Triton X-100, 150 mM NaCl, 1 mM $MgCl_2$, 1 mM sodium fluoride, 1 mM sodium orthovanadate, 1 mM β-glycerophosphate, and protease inhibitor cocktail; Roche). An equal amount of each protein lysate was incubated with anti-FLAG M2 Affinity Gel (Sigma-Aldrich) for 1 h at 4°C. The immune complexes and protein lysates were analyzed by Western blot with anti-LKB1 and anti-MO25 antibody. The immune complexes were in parallel subjected to liquid chromatography/tandem mass spectrometry (LC–MS/MS) analysis.

SDS-PAGE

For LC–MS/MS analysis, protein samples were boiled for 5 min and resolved in 12.5% acrylamide gels, using a Mini-Protean II electrophoresis cell (Bio-Rad). A constant voltage of 150 V was applied for 45 min. Gels were fixed in a solution containing 10% acetic acid and 40% ethanol for 30 min and stained overnight in Sypro Ruby (Bio-Rad). Gels were then washed in a solution containing 10% ethanol and 7% acetic acid for 30 min, and the image was acquired using a Typhoon Trio scanner (GE Healthcare). Each lane was cut in slices and subjected to tryptic digestion, followed by LC–MS/MS analysis.

Tryptic digestion

Gel bands were sliced into three small pieces, which were washed in milli-Q water. Reduction and alkylation were performed using 10 mM dithiothreitol in 50 mM ammonium bicarbonate at 56°C for 20 min, followed by iodoacetamide (50 mM iodoacetamide in 50 mM ammonium bicarbonate) for another 20 min in the dark. Gel pieces were dried and incubated with trypsin (12.5 µg/ml in 50 mM ammonium bicarbonate) for 20 min on ice. After rehydration, the trypsin supernatant was discarded. Gel pieces were hydrated with 50 mM ammonium bicarbonate and incubated overnight at 37°C. After digestion, acidic peptides were cleaned with trifluoroacetic acid 0.1% and dried in an RVC2 25 speedvac concentrator (Martin Christ). Peptides were resuspended in 10 µl of 0.1% fluoroacetic acid and sonicated for 5 min before analysis.

LC-MS analysis

LC was performed using an NanoAcquity nano-HPLC (Waters), equipped with a Waters BEH C18 nano-column (200 mm × 75 µm; internal diameter, 1.8 µm), A chromatographic ramp of 30 min (5–60% ACN) was used with a flow rate of 300 nl/min. Mobile phase A was water containing 0.1% vol/vol formic acid, and mobile phase B was ACN containing 0.1% vol/vol formic acid. A lock mass compound [Glu1]-fibrinopeptide B (100 fmol/µl) was delivered by an auxiliary pump of the LC system at 500 nl/min to the reference sprayer of the NanoLockSpray (Waters) source of the mass spectrometer.

LC was connected online to a Synapt G2Si electrospray ionization Q-Mobility-TOF mass spectrometer (Waters) equipped with an ion mobility chamber (T-Wave-IMS) for high-definition data acquisition analyses. All analyses were performed in positive-mode electrospray ionization. Data were postacquisition lock mass corrected using the double-charged monoisotopic ion of [Glu1]-fibrinopeptide B. Accurate mass LC-MS data were collected in hexadehydro-Diels–Alder mode, which enhances signal intensities using the ion mobility separation step.

Database searching was performed using Mascot 2.2.07 (Matrixscience) against a Uniprot-Swissprot database filled only with entries corresponding to *Homo sapiens* (without isoforms). For protein identification, the following parameters were adopted: carbamidomethylation of cysteines (C) as fixed modification, oxidation of methionines (M) as variable modification, 15 ppm of peptide mass tolerance, 0.2 D fragment mass tolerance, ≤3 missed cleavage points, and peptide charges of +2 and +3.

Progenesis LC-MS software analysis

Progenesis LC-MS (v2.0.5556.29015, Nonlinear Dynamics) was used for the label-free differential protein expression analysis. One of the runs was used as the reference to which the precursor masses in all other samples were aligned. Only features comprising charges of 2+ and 3+ were selected. The raw abundances of each feature were automatically normalized and logarithmized against the reference run. Samples were grouped in accordance to the comparison being performed, and ANOVA was performed. A peak list containing the information of all the features was generated and exported to the Mascot search engine (Matrix Science). This file was searched against a Uniprot/Swissprot database under the conditions stated in the previous section, and the list of identified peptides was imported back to Progenesis LC-MS. Protein quantitation was performed based on the three most intense nonconflicting peptides (peptides occurring in only one protein), except for proteins with only two nonconflicting peptides. The significance of expression changes was tested at the protein level, and proteins identified with at least two peptides, an ANOVA P value ≤0.05, and a ratio >1.5 in either direction were selected for further analyses.

Gene expression microarrays

Gene expression analysis of tumors from different mouse models (the original $Pten^{pc-/-}$ mouse model [Chen et al., 2005] versus the $Pten^{pc+/-}$ $Lkb1^{pc-/-}$ generated in this study) was performed using GeneChip Mouse Transcriptome Array 1.0 (Affymetrix). Differential expression was obtained using Transcriptome Analysis Console v4.0. Expression data were normalized and background- and batch-corrected using the Signal Space Transformation-Robust Multi-Chip Analysis implemented in that software. Data are deposited in GEO (GSE133837).

Downloaded from http://rupress.org/jem/article-pdf/217/6/e20191787/1780008/jem_20191787.pdf by guest on 09 February 2026

Total RNA was extracted from formalin-fixed and paraffin-embedded (FFPE) tissue using RNAstorm FFPE RNA extraction kit (Cell Data Sciences) according to the manufacturer's instructions. cDNAs from a total of 12 ng RNA were generated, fragmented, biotinylated, and hybridized to the GeneChip Mouse Transcriptome Array 1.0. The arrays were washed and stained on a GeneChip Fluidics Station 450 (Affymetrix); scanning was performed with the GeneChip Scanner 3000 7G and image analysis with the Affymetrix GeneChip Command Console Scan Control. Gene set enrichment analysis was performed using the MSigDB database (Subramanian et al., 2005).

Next-generation sequencing and copy number variation (CNV) calling

DNA was extracted from FFPE tumor blocks positive for tumor content using the FFPE Tissue DNA kit (Qiagen). DNA was quantified with the Quant-iT high-sensitivity PicoGreen double-stranded DNA Assay Kit (Invitrogen), and quality control was performed with the Illumina FFPE quality control kit (WG-321-1001). Libraries for next-generation targeted sequencing were constructed from 40 ng of DNA using a customized panel (Generead DNaseq Mix-n-Match Panel v2; Qiagen) as previously described (Mateo et al., 2015). CNVs were assessed from the aligned sequence files (.bam) using CNVkit v0.7.3 (Seed et al., 2017; Talevich et al., 2016; Turajlic et al., 2018).

Statistics and reproducibility

No statistical method was used to predetermine sample size. The experiments were not randomized. The investigators were not blinded to allocation during experiments and outcome assessment. *n* values represent the number of independent experiments performed, the number of individual mice, or the number of patient specimens. Unless otherwise stated, data analyzed by parametric tests are represented by the mean ± SEM of pooled experiments and the median ± interquartile range for experiments analyzed by nonparametric tests. For each independent in vitro experiment, at least three technical replicates were used, and a minimum number of three experiments was performed to ensure adequate statistical power. In the in vitro experiments, normal distribution was assumed, and one-sample *t* tests were applied for one-component comparisons with control and Student's *t* test for two-component comparisons. For in vivo experiments, D'Agostino–Pearson, Shapiro–Wilk, and Kolmogorov–Smirnov normality tests were applied. Student's *t* test was used to compare data with normal distribution, and nonparametric Mann–Whitney *U* exact test was used to analyze samples not following a normal distribution. The confidence level used for all the statistical analyses was 95% ($\alpha = 0.05$). Two-tailed statistical analysis was applied for experimental design without predicted result, and one-tailed for validation or hypothesis-driven experiments. GraphPad Prism 8.0.2 software was used for statistical calculations.

Acknowledgments

We are grateful to the Carracedo laboratory for valuable input and to Diego Barriales, Elisabet Megias-Roda, Juan Anguita, David Barneda, Len Stephens, Ana M. Aransay, and Felix Elortza for technical advice.

I. Hermanova and F. Salvador were funded by the Juan de la Cierva program from the Spanish Ministry of Research. V. Torrano is funded by Fundación Vasca de Innovación e Investigación Sanitarias, Bioef (BIO15/CA/052), the Ministerio de Ciencia, Innovación y Universidades (RTI2018-097267-B-100), the Fundación Científica Asociación Española Contra el Cáncer J.P. Bizkaia, and the Basque Department of Health (2016111109). The work of A. Carracedo is supported by the Basque Department of Industry, Tourism and Trade (Elkartek), the Department of Education (IKERTALDE IT1106-16, with A. Gomez-Muñoz), the Department of Health (2019222031), the Fundación BBVA, the Ministerio de Ciencia, Innovación y Universidades (SAF2016-79381-R, FEDER [European Regional Development Fund, EU]; Severo Ochoa Excellence Accreditation SEV-2016-0644; Excellence Networks SAF2016-81975-REDT), European Training Networks Project (H2020-MSCA-ITN-308 2016 721532, with G. Velasco), the Fundación Científica Asociación Española Contra el Cáncer (IDEAS175CARR; GCTRA18006CARR, with M. Graupera and R.R. Gomis), "La Caixa" Foundation (HR17-00094), and the European Research Council (Starting Grant 336343, PoC 754627, and Consolidator Grant 819242). We are grateful for the support of Mondravember and Movembergara. J.M. Paramio was funded by Ministerio de Ciencia, Innovación y Universidades (SAF2015-66015-R and CB16/12/00228). J.I. López was funded by the Ministerio de Ciencia, Innovación y Universidades (SAF2016-79847-R). R. Barrio and J.D. Sutherland acknowledge Ministerio de Ciencia, Innovación y Universidades/European Regional Development Fund (BFU2017-84653-P, SEV-2016-0644). G. Velasco's research is supported by grants integrated into the State Plan for R & D + I2013-2016 and funded by the Instituto de Salud Carlos III (PI18/00442 and PI15/00339), the European Regional Development Fund, and Fundació la Marató de TV3 (20134031). J.M. Lizcano was supported by the Ministerio de Ciencia, Innovación y Universidades (SAF2015-64237-R) and cofunded by the European Regional Development Fund. R.R. Gomis is supported by the Ministerio de Ciencia, Innovación y Universidades, European Regional Development Fund (CIBERONC and SAF016-76008R), and "La Caixa" Foundation (HR17-00092). CIBERONC was cofunded with European Regional Development funds and funded by Instituto de Salud Carlos III. L. Valcarcel-Jimenez was funded by a Basque Government predoctoral grant.

Author contributions: In vitro studies: I. Hermanova, P. Zúñiga-García, and A. Caro-Maldonado, with support from S. Fernandez-Rui, N. Martín-Martín, A. Arruabarrena-Aristorena, L. Valcarcel-Jimenez, and A. Talamillo. In vivo studies: I. Hermanova, P. Zúñiga-García, A. Caro-Maldonado, and M. Nuñez-Olle, with support from N. Martín-Martín, A. Zabala-Letona, A. Carracedo, M. Lorente, M. Guiu, and V. Torrano. In vivo bioluminescence assays: F. Salvador and R.R. Gomis. Genotyping and cloning: I. Astobiza and S. Fernandez-Rui, with support from J.D. Sutherland and R. Barrio. Pathologic and immunohistochemical analysis of murine tissues: J.M. Flores and J.I. López, with participation of I. Hermanova, I. Lodewijk, C. Suárez-Cabrera, S. Fernandez-Rui, and L. Camacho for immunohistochemistry. Pathologic, genetic, and immunohistochemical analysis of

Downloaded from http://rupress.org/jem/article-pdf/217/6/e20191787/1780008/jem_20191787.pdf by guest on 09 February 2026

human PCa specimens: B. Gurel and S. Carreira, supervised by J.S. de Bono. Immunofluorescence analysis of tissues: A. Martinez-Romero, supervised by M. Graupera. LKB1 kinase radiochemical assay: J.M. Lizcano. Bioinformatics and statistical analysis: A.R. Cortazar. Murine tissue microdissection and gene expression analysis: C. Suárez-Cabrera, I. Lodewijk, and J.M. Paramio. Other contributions: G. Velasco (supervision in xenograft experiments), A. Gomez-Muñoz (shared supervision of L. Camacho), J. Trka (shared supervision of I. Hermanova), V. Torrano (support with human cancer dataset analysis). General supervision of data analysis, project direction, and manuscript writing: A. Carracedo.

Disclosures: Dr. Graupera reported, "the Graupera laboratory has research agreements with ArQule and Venthera. None of those have a relationship with cancer or LKB1." Dr. Gomis reported shares of Inbiomotion (<$10,000). No other disclosures were reported.

Submitted: 23 September 2019
Revised: 16 December 2019
Accepted: 6 February 2020

References

Abida, W., J. Armenia, A. Gopalan, R. Brennan, M. Walsh, D. Barron, D. Danila, D. Rathkopf, M. Morris, S. Slovin, et al. 2017. Prospective Genomic Profiling of Prostate Cancer Across Disease States Reveals Germline and Somatic Alterations That May Affect Clinical Decision Making. *JCO Precis. Oncol.* 2017:PO.17.00029.

Abida, W., J. Cyrta, G. Heller, D. Prandi, J. Armenia, I. Coleman, M. Cieslik, M. Benelli, D. Robinson, E.M. Van Allen, et al. 2019. Genomic correlates of clinical outcome in advanced prostate cancer. *Proc. Natl. Acad. Sci. USA.* 116:11428–11436. https://doi.org/10.1073/pnas.1902651116

Agarwal, S., P.G. Hynes, H.S. Tillman, R. Lake, W.G. Abou-Kheir, L. Fang, O.M. Casey, A.H. Ameri, P.L. Martin, J.J. Yin, et al. 2015. Identification of Different Classes of Luminal Progenitor Cells within Prostate Tumors. *Cell Rep.* 13:2147–2158. https://doi.org/10.1016/j.celrep.2015.10.077

Alimonti, A., A. Carracedo, J.G. Clohessy, L.C. Trotman, C. Nardella, A. Egia, L. Salmena, K. Sampieri, W.J. Haveman, E. Brogi, et al. 2010. Subtle variations in Pten dose determine cancer susceptibility. *Nat. Genet.* 42: 454–458. https://doi.org/10.1038/ng.556

Armenia, J., S.A.M. Wankowicz, D. Liu, J. Gao, R. Kundra, E. Reznik, W.K. Chatila, D. Chakravarty, G.C. Han, I. Coleman, et al. PCF/SU2C International Prostate Cancer Dream Team. 2018. The long tail of oncogenic drivers in prostate cancer. *Nat. Genet.* 50:645–651. https://doi.org/10.1038/s41588-018-0078-z

Arriaga, J.M., and C. Abate-Shen. 2019. Genetically Engineered Mouse Models of Prostate Cancer in the Postgenomic Era. *Cold Spring Harb. Perspect. Med.* 9:a030528. https://doi.org/10.1101/cshperspect.a030528

Berger, A.H., A.G. Knudson, and P.P. Pandolfi. 2011. A continuum model for tumour suppression. *Nature.* 476:163–169. https://doi.org/10.1038/nature10275

Boudeau, J., M. Deak, M.A. Lawlor, N.A. Morrice, and D.R. Alessi. 2003. Heat-shock protein 90 and Cdc37 interact with LKB1 and regulate its stability. *Biochem. J.* 370:849–857. https://doi.org/10.1042/bj20021813

Brunnhoelzl, D., and J. Wang. 2018. Clinical features, treatment, prognosis, and outcome of 47 patients with pure squamous cell carcinoma of the prostate. *J. Clin. Oncol.* 36(6 suppl):7. https://doi.org/10.1200/JCO.2018.36.6_suppl.7

Cancer Genome Atlas Research Network. 2015. The Molecular Taxonomy of Primary Prostate Cancer. *Cell.* 163:1011–1025. https://doi.org/10.1016/j.cell.2015.10.025

Carracedo, A., D. Weiss, A.K. Leliaert, M. Bhasin, V.C. de Boer, G. Laurent, A.C. Adams, M. Sundvall, S.J. Song, K. Ito, et al. 2012. A metabolic prosurvival role for PML in breast cancer. *J. Clin. Invest.* 122:3088–3100. https://doi.org/10.1172/JCI62129

Cerami, E., J. Gao, U. Dogrusoz, B.E. Gross, S.O. Sumer, B.A. Aksoy, A. Jacobsen, C.J. Byrne, M.L. Heuer, E. Larsson, et al. 2012. The cBio cancer genomics portal: an open platform for exploring multidimensional cancer genomics data. *Cancer Discov.* 2:401–404. https://doi.org/10.1158/2159-8290.CD-12-0095

Chang, A.J., K.A. Autio, M. Roach III, and H.I. Scher. 2014. High-risk prostate cancer-classification and therapy. *Nat. Rev. Clin. Oncol.* 11:308–323. https://doi.org/10.1038/nrclinonc.2014.68

Chen, Z., L.C. Trotman, D. Shaffer, H.K. Lin, Z.A. Dotan, M. Niki, J.A. Koutcher, H.I. Scher, T. Ludwig, W. Gerald, et al. 2005. Crucial role of p53-dependent cellular senescence in suppression of Pten-deficient tumorigenesis. *Nature.* 436:725–730. https://doi.org/10.1038/nature03918

Di Cristofano, A., B. Pesce, C. Cordon-Cardo, and P.P. Pandolfi. 1998. Pten is essential for embryonic development and tumour suppression. *Nat. Genet.* 19:348–355. https://doi.org/10.1038/1235

Ferraldeschi, R., D. Nava Rodrigues, R. Riisnaes, S. Miranda, I. Figueiredo, P. Rescigno, P. Ravi, C. Pezaro, A. Omlin, D. Lorente, et al. 2015. PTEN protein loss and clinical outcome from castration-resistant prostate cancer treated with abiraterone acetate. *Eur. Urol.* 67:795–802. https://doi.org/10.1016/j.eururo.2014.10.027

Fraser, M., V.Y. Sabelnykova, T.N. Yamaguchi, L.E. Heisler, J. Livingstone, V. Huang, Y.J. Shiah, F. Yousif, X. Lin, A.P. Masella, et al. 2017. Genomic hallmarks of localized, non-indolent prostate cancer. *Nature.* 541: 359–364. https://doi.org/10.1038/nature20788

Gao, J., B.A. Aksoy, U. Dogrusoz, G. Dresdner, B. Gross, S.O. Sumer, Y. Sun, A. Jacobsen, R. Sinha, E. Larsson, et al. 2013. Integrative analysis of complex cancer genomics and clinical profiles using the cBioPortal. *Sci. Signal.* 6:pl1. https://doi.org/10.1126/scisignal.2004088

Gerhauser, C., F. Favero, T. Risch, R. Simon, L. Feuerbach, Y. Assenov, D. Heckmann, N. Sidiropoulos, S.M. Waszak, D. Hübschmann, et al. 2018. Molecular Evolution of Early-Onset Prostate Cancer Identifies Molecular Risk Markers and Clinical Trajectories. *Cancer Cell.* 34:996–1011.e8. https://doi.org/10.1016/j.ccell.2018.10.016

Hollstein, P.E., L.J. Eichner, S.N. Brun, A. Kamireddy, R.U. Svensson, L.I. Vera, D.S. Ross, T.J. Rymoff, A. Hutchins, H.M. Galvez, et al. 2019. The AMPK-related kinases SIK1 and SIK3 mediate key tumor-suppressive effects of LKB1 in NSCLC. *Cancer Discov.* 9:1606–1627. https://doi.org/10.1158/2159-8290.CD-18-1261

Huang, X., S. Wullschleger, N. Shpiro, V.A. McGuire, K. Sakamoto, Y.L. Woods, W. McBurnie, S. Fleming, and D.R. Alessi. 2008. Important role of the LKB1-AMPK pathway in suppressing tumorigenesis in PTEN-deficient mice. *Biochem. J.* 412:211–221. https://doi.org/10.1042/BJ20080557

Ikediobi, O.N., H. Davies, G. Bignell, S. Edkins, C. Stevens, S. O'Meara, T. Santarius, T. Avis, S. Barthorpe, L. Brackenbury, et al. 2006. Mutation analysis of 24 known cancer genes in the NCI-60 cell line set. *Mol. Cancer Ther.* 5:2606–2612. https://doi.org/10.1158/1535-7163.MCT-06-0433

Imielinski, M., A.H. Berger, P.S. Hammerman, B. Hernandez, T.J. Pugh, E. Hodis, J. Cho, J. Suh, M. Capelletti, A. Sivachenko, et al. 2012. Mapping the hallmarks of lung adenocarcinoma with massively parallel sequencing. *Cell.* 150:1107–1120. https://doi.org/10.1016/j.cell.2012.08.029

Ireland, H., R. Kemp, C. Houghton, L. Howard, A.R. Clarke, O.J. Sansom, and D.J. Winton. 2004. Inducible Cre-mediated control of gene expression in the murine gastrointestinal tract: effect of loss of beta-catenin. *Gastroenterology.* 126:1236–1246. https://doi.org/10.1053/j.gastro.2004.03.020

Ittmann, M., J. Huang, E. Radaelli, P. Martin, S. Signoretti, R. Sullivan, B.W. Simons, J.M. Ward, B.D. Robinson, G.C. Chu, et al. 2013. Animal models of human prostate cancer: the consensus report of the New York meeting of the Mouse Models of Human Cancers Consortium Prostate Pathology Committee. *Cancer Res.* 73:2718–2736. https://doi.org/10.1158/0008-5472.CAN-12-4213

James, N.D., M.R. Spears, N.W. Clarke, D.P. Dearnaley, J.S. De Bono, J. Gale, J. Hetherington, P.J. Hoskin, R.J. Jones, R. Laing, et al. 2015. Survival with Newly Diagnosed Metastatic Prostate Cancer in the "Docetaxel Era": Data from 917 Patients in the Control Arm of the STAMPEDE Trial (MRC PR08, CRUK/06/019). *Eur. Urol.* 67:1028–1038. https://doi.org/10.1016/j.eururo.2014.09.032

Jordan, E.J., H.R. Kim, M.E. Arcila, D. Barron, D. Chakravarty, J. Gao, M.T. Chang, A. Ni, R. Kundra, P. Jonsson, et al. 2017. Prospective Comprehensive Molecular Characterization of Lung Adenocarcinomas for Efficient Patient Matching to Approved and Emerging Therapies. *Cancer Discov.* 7:596–609. https://doi.org/10.1158/2159-8290.CD-16-1337

Downloaded from http://rupress.org/jem/article-pdf/217/6/e20191787/1780008/jem_20191787.pdf by guest on 09 February 2026

Knudson, A.G. Jr. 1971. Mutation and cancer: statistical study of retinoblastoma. *Proc. Natl. Acad. Sci. USA.* 68:820–823. https://doi.org/10.1073/pnas.68.4.820

Kumar, A., I. Coleman, C. Morrissey, X. Zhang, L.D. True, R. Gulati, R. Etzioni, H. Bolouri, B. Montgomery, T. White, et al. 2016. Substantial interindividual and limited intraindividual genomic diversity among tumors from men with metastatic prostate cancer. *Nat. Med.* 22:369–378. https://doi.org/10.1038/nm.4053

Li, G., G.W. Robinson, R. Lesche, H. Martinez-Diaz, Z. Jiang, N. Rozengurt, K.U. Wagner, D.C. Wu, T.F. Lane, X. Liu, et al. 2002. Conditional loss of PTEN leads to precocious development and neoplasia in the mammary gland. *Development*. 129:4159–4170.

Lizcano, J.M., O. Göransson, R. Toth, M. Deak, N.A. Morrice, J. Boudeau, S.A. Hawley, L. Udd, T.P. Mäkelä, D.G. Hardie, and D.R. Alessi. 2004. LKB1 is a master kinase that activates 13 kinases of the AMPK subfamily, including MARK/PAR-1. *EMBO J.* 23:833–843. https://doi.org/10.1038/sj.emboj.7600110

Martin, P., Y.N. Liu, R. Pierce, W. Abou-Kheir, O. Casey, V. Seng, D. Camacho, R.M. Simpson, and K. Kelly. 2011. Prostate epithelial Pten/TP53 loss leads to transformation of multipotential progenitors and epithelial to mesenchymal transition. *Am. J. Pathol.* 179:422–435. https://doi.org/10.1016/j.ajpath.2011.03.035

Martín-Martín, N., A. Zabala-Letona, S. Fernández-Ruiz, L. Arreal, L. Camacho, M. Castillo-Martin, A.R. Cortazar, V. Torrano, I. Astobiza, P. Zúñiga-García, et al. 2018. PPARδ Elicits Ligand-Independent Repression of Trefoil Factor Family to Limit Prostate Cancer Growth. *Cancer Res.* 78:399–409. https://doi.org/10.1158/0008-5472.CAN-17-0908

Mateo, J., S. Carreira, S. Sandhu, S. Miranda, H. Mossop, R. Perez-Lopez, D. Nava Rodrigues, D. Robinson, A. Omlin, N. Tunariu, et al. 2015. DNA-Repair Defects and Olaparib in Metastatic Prostate Cancer. *N. Engl. J. Med.* 373:1697–1708. https://doi.org/10.1056/NEJMoa1506859

Momcilovic, M., and D.B. Shackelford. 2015. Targeting LKB1 in cancer - exposing and exploiting vulnerabilities. *Br. J. Cancer.* 113:574–584. https://doi.org/10.1038/bjc.2015.261

Morgenstern, J.P., and H. Land. 1990. Advanced mammalian gene transfer: high titre retroviral vectors with multiple drug selection markers and a complementary helper-free packaging cell line. *Nucleic Acids Res.* 18:3587–3596. https://doi.org/10.1093/nar/18.12.3587

Munoz, F., P. Franco, P. Ciammella, M. Clerico, M. Giudici, A.R. Filippi, and U. Ricardi. 2007. Squamous cell carcinoma of the prostate: long-term survival after combined chemo-radiation. *Radiat. Oncol.* 2:15. https://doi.org/10.1186/1748-717X-2-15

Murray, C.W., J.J. Brady, M.K. Tsai, C. Li, I.P. Winters, R. Tang, L. Andrejka, R.K. Ma, C.A. Kunder, P. Chu, and M.M. Winslow. 2019. An Lkb1-Sik axis suppresses lung tumor growth and controls differentiation. *Cancer Discov.* 9:1590–1605. https://doi.org/10.1158/2159-8290.CD-18-1237

Nardella, C., A. Carracedo, L. Salmena, and P.P. Pandolfi. 2010. Faithfull modeling of PTEN loss driven diseases in the mouse. *Curr. Top. Microbiol. Immunol.* 347:135–168.

Pearson, H.B., A. McCarthy, C.M. Collins, A. Ashworth, and A.R. Clarke. 2008. Lkb1 deficiency causes prostate neoplasia in the mouse. *Cancer Res.* 68:2223–2232. https://doi.org/10.1158/0008-5472.CAN-07-5169

Seed, G., W. Yuan, J. Mateo, S. Carreira, C. Bertan, M. Lambros, G. Boysen, R. Ferraldeschi, S. Miranda, I. Figueiredo, et al. 2017. Gene Copy Number Estimation from Targeted Next-Generation Sequencing of Prostate Cancer Biopsies: Analytic Validation and Clinical Qualification. *Clin. Cancer Res.* 23:6070–6077. https://doi.org/10.1158/1078-0432.CCR-17-0972

Shappell, S.B., G.V. Thomas, R.L. Roberts, R. Herbert, M.M. Ittmann, M.A. Rubin, P.A. Humphrey, J.P. Sundberg, N. Rozengurt, R. Barrios, et al. 2004. Prostate pathology of genetically engineered mice: definitions and classification. The consensus report from the Bar Harbor meeting of the Mouse Models of Human Cancer Consortium Prostate Pathology Committee. *Cancer Res.* 64:2270–2305. https://doi.org/10.1158/0008-5472.CAN-03-0946

Shaw, R.J., N. Bardeesy, B.D. Manning, L. Lopez, M. Kosmatka, R.A. DePinho, and L.C. Cantley. 2004. The LKB1 tumor suppressor negatively regulates mTOR signaling. *Cancer Cell.* 6:91–99. https://doi.org/10.1016/j.ccr.2004.06.007

Stambolic, V., M.S. Tsao, D. Macpherson, A. Suzuki, W.B. Chapman, and T.W. Mak. 2000. High incidence of breast and endometrial neoplasia resembling human Cowden syndrome in pten+/- mice. *Cancer Res.* 60:3605–3611.

Stewart, S.A., D.M. Dykxhoorn, D. Palliser, H. Mizuno, E.Y. Yu, D.S. An, D.M. Sabatini, I.S. Chen, W.C. Hahn, P.A. Sharp, et al. 2003. Lentivirus-delivered stable gene silencing by RNAi in primary cells. *RNA.* 9:493–501. https://doi.org/10.1261/rna.2192803

Subramanian, A., P. Tamayo, V.K. Mootha, S. Mukherjee, B.L. Ebert, M.A. Gillette, A. Paulovich, S.L. Pomeroy, T.R. Golub, E.S. Lander, and J.P. Mesirov. 2005. Gene set enrichment analysis: a knowledge-based approach for interpreting genome-wide expression profiles. *Proc. Natl. Acad. Sci. USA.* 102:15545–15550. https://doi.org/10.1073/pnas.0506580102

Talevich, E., A.H. Shain, T. Botton, and B.C. Bastian. 2016. CNVkit: Genome-Wide Copy Number Detection and Visualization from Targeted DNA Sequencing. *PLOS Comput. Biol.* 12:e1004873. https://doi.org/10.1371/journal.pcbi.1004873

Taylor, B.S., N. Schultz, H. Hieronymus, A. Gopalan, Y. Xiao, B.S. Carver, V.K. Arora, P. Kaushik, E. Cerami, B. Reva, et al. 2010. Integrative genomic profiling of human prostate cancer. *Cancer Cell.* 18:11–22. https://doi.org/10.1016/j.ccr.2010.05.026

Torrano, V., L. Valcarcel-Jimenez, A.R. Cortazar, X. Liu, J. Urosevic, M. Castillo-Martin, S. Fernández-Ruiz, G. Morciano, A. Caro-Maldonado, M. Guiu, et al. 2016. The metabolic co-regulator PGC1α suppresses prostate cancer metastasis. *Nat. Cell Biol.* 18:645–656. https://doi.org/10.1038/ncb3357

Trotman, L.C., M. Niki, Z.A. Dotan, J.A. Koutcher, A. Di Cristofano, A. Xiao, A.S. Khoo, P. Roy-Burman, N.M. Greenberg, T. Van Dyke, et al. 2003. Pten dose dictates cancer progression in the prostate. *PLoS Biol.* 1:E59. https://doi.org/10.1371/journal.pbio.0000059

Turajlic, S., H. Xu, K. Litchfield, A. Rowan, T. Chambers, J.I. Lopez, D. Nicol, T. O'Brien, J. Larkin, S. Horswell, et al. TRACERx Renal Consortium. 2018. Tracking Cancer Evolution Reveals Constrained Routes to Metastases: TRACERx Renal. *Cell.* 173:581–594.e12. https://doi.org/10.1016/j.cell.2018.03.057

Ugalde-Olano, A., A. Egia, S. Fernández-Ruiz, A. Loizaga-Iriarte, P. Zuñiga-García, S. Garcia, F. Royo, I. Lacasa-Viscasillas, E. Castro, A.R. Cortazar, et al. 2015. Methodological aspects of the molecular and histological study of prostate cancer: focus on PTEN. *Methods.* 77-78:25–30. https://doi.org/10.1016/j.ymeth.2015.02.005

Weinstein, J.N., E.A. Collisson, G.B. Mills, K.R. Shaw, B.A. Ozenberger, K. Ellrott, I. Shmulevich, C. Sander, and J.M. Stuart. Cancer Genome Atlas Research Network. 2013. The Cancer Genome Atlas Pan-Cancer analysis project. *Nat. Genet.* 45:1113–1120. https://doi.org/10.1038/ng.2764

Xie, Q., Y. Liu, T. Cai, C. Horton, J. Stefanson, and Z.A. Wang. 2017. Dissecting cell-type-specific roles of androgen receptor in prostate homeostasis and regeneration through lineage tracing. *Nat. Commun.* 8:14284. https://doi.org/10.1038/ncomms14284

Xu, C., C.M. Fillmore, S. Koyama, H. Wu, Y. Zhao, Z. Chen, G.S. Herter-Sprie, E.A. Akbay, J.H. Tchaicha, A. Altabef, et al. 2014. Loss of Lkb1 and Pten leads to lung squamous cell carcinoma with elevated PD-L1 expression. *Cancer Cell.* 25:590–604. https://doi.org/10.1016/j.ccr.2014.03.033

Downloaded from http://rupress.org/jem/article-pdf/217/6/e20191787/1780008/jem_20191787.pdf by guest on 09 February 2026

JEM

Supplemental material

Downloaded from http://rupress.org/jem/article-pdf/217/6/e20191787/1780008/jem_20191787.pdf by guest on 09 February 2026

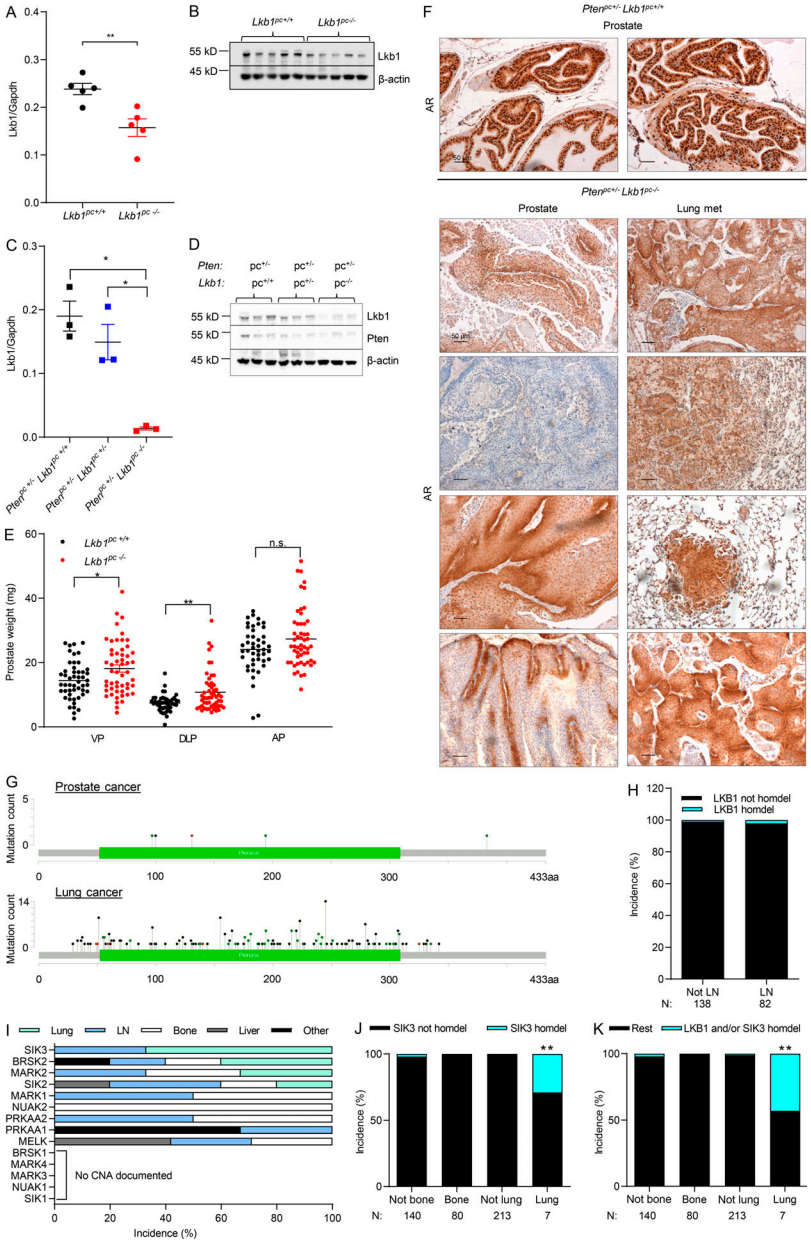

Figure S1. **Consequences of aberrations in Lkb1 or its targets in murine and human prostate tissue. (A)** Analysis of *Lkb1* gene expression by qRT-PCR in $Lkb1^{pc+/+}$ (n = 5) and $Lkb1^{pc-/-}$ (n = 5) mice. Data were normalized to *Gapdh* expression. **(B)** Western blot analysis for Lkb1 protein expression in $Lkb1^{pc+/+}$ (n = 5) and $Lkb1^{pc-/-}$ (n = 5) mice. **(C)** Analysis of *Lkb1* gene expression by qRT-PCR in $Pten^{pc+/-}$ $Lkb1^{pc+/+}$ (n = 3), $Pten^{pc+/-}$ $Lkb1^{pc+/-}$ (n = 3), and $Pten^{pc+/-}$ $Lkb1^{pc-/-}$ (n = 3) mice. Data are normalized to *Gapdh* expression. **(D)** Western blot analysis of Lkb1 and Pten protein expression in $Pten^{pc+/-}$ $Lkb1^{pc+/+}$ (n = 3), $Pten^{pc+/-}$ $Lkb1^{pc+/-}$ (n = 3), and $Pten^{pc+/-}$ $Lkb1^{pc-/-}$ (n = 3) mice. **(E)** Quantification of ventral (VP), dorsolateral (DLP) and anterior (AP) prostate weight in $Lkb1^{pc+/+}$ and $Lkb1^{pc-/-}$ mice (n = 27; two lobes per mouse). **(F)** Immunohistochemical images of AR staining in prostate tissue in $Pten^{pc+/-}$ $Lkb1^{pc+/+}$ mice (upper panels) and prostate tumors and lung metastatic lesions in $Pten^{pc+/-}$ $Lkb1^{pc-/-}$ mice (lower panels). **(G)** Lollipop representation of *LKB1* point mutations in PCa (Abida et al., 2017; Abida et al., 2019; Armenia et al., 2018; Cancer Genome Atlas Research Network, 2015; Fraser et al., 2017; Gerhauser et al., 2018; Kumar et al., 2016; Taylor et al., 2010) and lung adenocarcinoma (Imielinski et al., 2012; Weinstein et al., 2013; Jordan et al., 2017) datasets. **(H)** Incidence of *LKB1* genomic alterations in metastatic specimens of patients with metastatic PCa (Armenia et al., 2018). Cases without *LKB1* homozygous deletion (*LKB1* not homdel); cases with *LKB1* homozygous deletion (homdel). Not LN, metastasis identified in all analyzed tissues except for lymph node. Numbers below the graph indicate total number of analyzed metastatic samples. **(I)** Incidence of genomic aberrations in metastatic lesions in lung, lymph nodes, bone, liver, and other tissues in patients with metastatic PCa for the indicated genes (LKB1 targets; Armenia et al., 2018). **(J)** Incidence of *LKB1* genomic alterations in metastatic specimens of patients with metastatic PCa (Armenia et al., 2018). Cases without *SIK3* homozygous deletion (*SIK3* not homdel); cases with *SIK3* homozygous deletion (homdel). Not bone, metastasis identified in all analyzed tissues except for bone; not lung, metastasis identified in all analyzed tissues except for lung. Numbers below the graph indicate total number of analyzed metastatic samples. **(K)** Incidence of *LKB1* and/or *SIK3* genomic alterations in metastatic specimens of patients with metastatic PCa (Armenia et al., 2018). Cases without *LKB1* and/or *SIK3* homozygous deletion (*Rest*); cases with *LKB1* and/or *SIK3* homozygous deletion (homdel). Not bone, metastasis identified in all analyzed tissues except for bone; not lung, metastasis identified in all analyzed tissues except for lung. Numbers below the graph indicate total number of analyzed metastatic samples. Statistic tests: one-tailed Mann–Whitney test (A, C, and E); Fisher exact test (J and K). n.s., not significant; *, P < 0.05; **, P < 0.01. Error bars represent SEM.

Downloaded from http://rupress.org/jem/article-pdf/217/6/e20191787/1780008/jem_20191787.pdf by guest on 09 February 2026

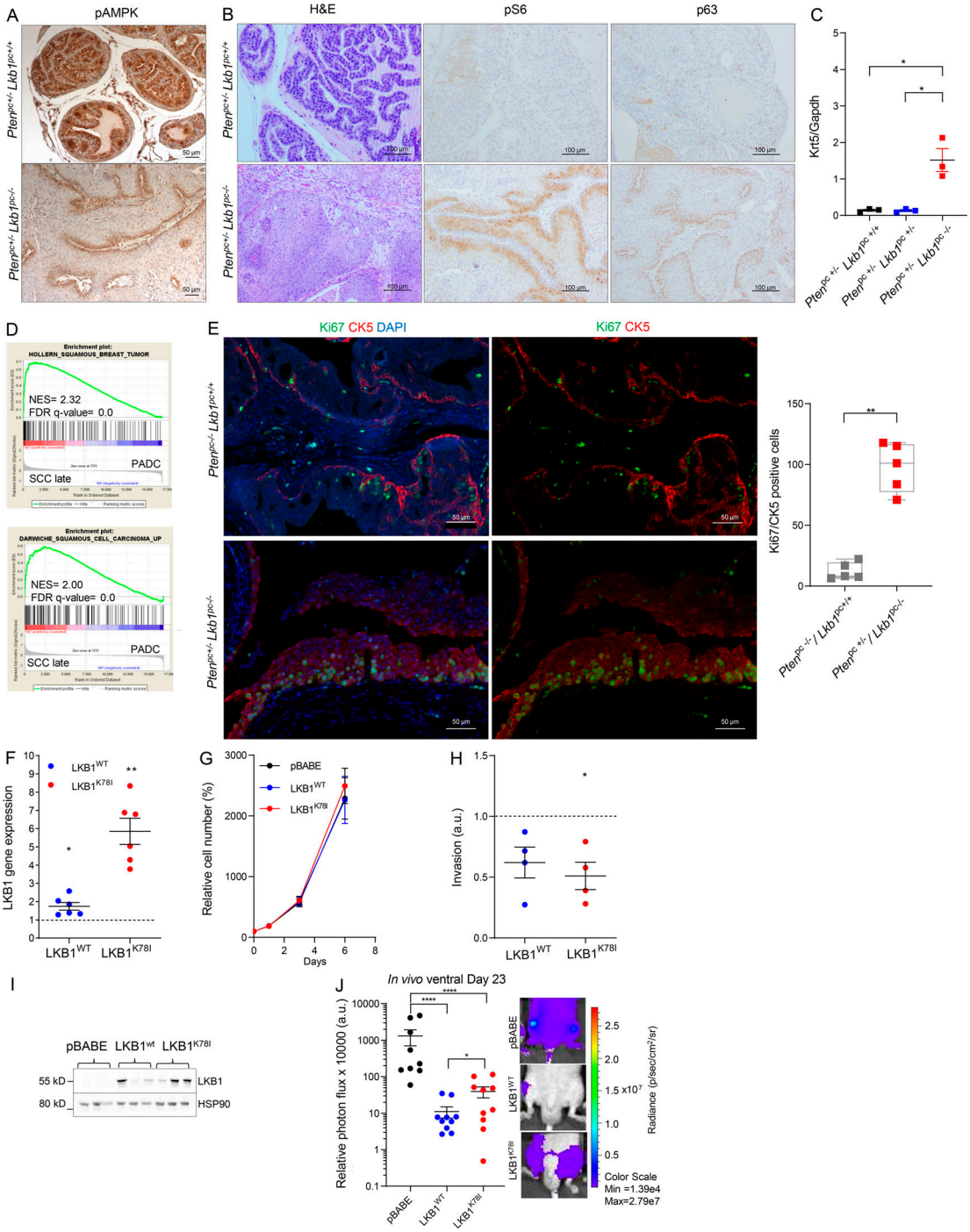

Figure S2. **Pathological and molecular characterization of *Lkb1* perturbations in murine and human prostate cells. (A)** Immunohistochemical images of prostate tissue in *Pten*$^{pc+/-}$ *Lkb1*$^{pc+/+}$ and *Pten*$^{pc+/-}$ *Lkb1*$^{pc-/-}$ mice. Staining as indicated: p-AMPK (Thr172). **(B)** Representative immunohistochemical images of prostate tissue in *Pten*$^{pc+/-}$ *Lkb1*$^{pc+/+}$ and *Pten*$^{pc+/-}$ *Lkb1*$^{pc-/-}$ mice. Staining as indicated: H&E, pS6 (Ser235/236), and p63. **(C)** Analysis of *Krt5* gene expression by qRT-PCR in *Pten*$^{pc+/-}$ *Lkb1*$^{pc+/+}$ (n = 3), *Pten*$^{pc+/-}$ *Lkb1*$^{pc+/-}$ (n = 3), and *Pten*$^{pc+/-}$ *Lkb1*$^{pc-/-}$ (n = 3) mice. Data are normalized to *Gapdh* expression. **(D)** Gene set enrichment analysis of the squamous cell carcinoma signature in *Pten*$^{pc+/-}$ *Lkb1*$^{pc-/-}$ (SCC-squamous cell carcinoma) and Pten$^{pc-/-}$ *Lkb1*$^{pc+/+}$ (PADC-prostate adenocarcinoma) mice. **(E)** Representative immunofluorescence images (left) of Ki67 (green) and CK5 (red), with quantification of double positive cells (right) in prostate tissue of Pten$^{pc-/-}$ *Lkb1*$^{pc+/+}$ and *Pten*$^{pc+/-}$ *Lkb1*$^{pc-/-}$ mice. **(F)** Analysis of *LKB1* gene expression by qRT-PCR in DU145 cells with ectopic expression of WT LKB1 (LKB1^{WT}), the kinase-defective LKB1-K78I mutant (LKB1^{K78I}), or transduced with mock vector (pBABE; n = 6; independent experiments). Data are normalized to control (pBABE; dashed line). **(G)** Effect of LKB1^{WT}and LKB1^{K78I} expression on cellular growth (n = 3; independent experiments). **(H)** Quantification of invasion (C; n = 4, independent experiments) in LKB1^{WT}, the LKB1^{K78I}, or pBABE-transduced DU145 cells. Data are normalized to control (pBABE; dashed line). **(I)** Western blot analysis for LKB1 protein expression in harvested xenograft tumors (n = 3 samples per condition). **(J)** Metastatic capacity of control (pBABE) and LKB1^{WT}- and LKB1^{K78I}-expressing DU145 cells using intracardiac xenotransplant assays. Quantification (left) and representative ventral view (right) of luciferase-dependent signal intensity of DU145 cells captured on day 23. Statistic tests: one-tailed Mann–Whitney test (C, E, and J); one-sample t test (F and H); *, P < 0.05; **, P < 0.01; ****, P < 0.0001. Error bars represent SEM.

Downloaded from http://rupress.org/jem/article-pdf/217/6/e20191787/1780008/jem_20191787.pdf by guest on 09 February 2026

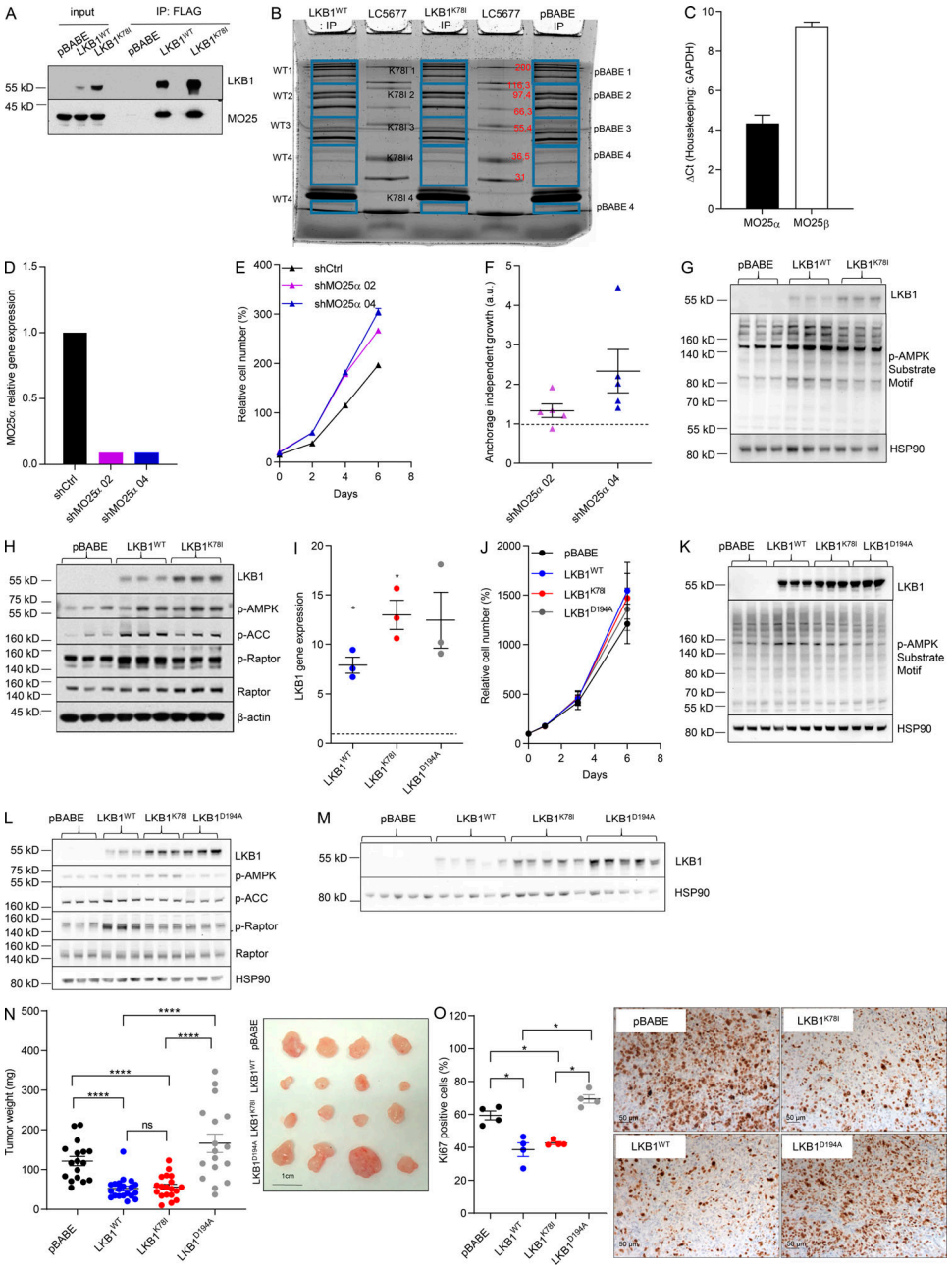

Figure S3. **Molecular analysis of LKB1 reexpression in human PCa cells. (A)** Western blot analysis for LKB1 and MO25 protein expression of input and flag immunoprecipitates in DU145 cell line with ectopic expression of Flag-tagged LKB1^{WT} and LKB1^{K78I}. **(B)** Picture of SDS-PAGE gel with separation of immunoprecipitated proteins. Blue squares indicate areas selected for subsequent LC-MS–based identification and quantitation. **(C)** Representative analysis of relative *MO25α* and *MO25β* mRNA abundance by qRT-PCR in DU145 cells (n = 3). **(D)** Representative analysis of *MO25α* gene expression by qRT-PCR in DU145 cells transduced with scramble shRNA (shCtrl) or two independent shRNA (shMO25α 02; shMO25α 04; n = 3). **(E and F)** Effect of *MO25α* gene silencing on cellular growth (E; n = 3; independent experiments) and anchorage independent growth (F; n = 5; independent experiments; data are normalized to control; shCtrl, dashed line). **(G)** Representative Western blot analysis using AMPK motif antibody in control and LKB1^{WT}- and LKB1^{K78I}-expressing cells (n = 3). **(H)** Representative Western blot analysis of LKB1, p-AMPK, p-ACC, p-Raptor, Raptor, and β-actin protein expression in control and LKB1^{WT}- and LKB1^{K78I}-expressing cells (n = 5). **(I)** Analysis of *LKB1* gene expression by qRT-PCR in DU145 cells with ectopic expression of LKB1^{WT}, LKB1^{K78I}, and LKB1^{D194A} or transduced with mock vector (pBABE; n = 3; independent experiments). Data are normalized to control (pBABE; dashed line). **(J)** Effect of LKB1^{WT}, LKB1^{K78I}, and LKB1^{D194A} expression on cell growth (n = 3; independent experiments). **(K)** Western blot analysis using AMPK motif antibody in control and LKB1^{WT}-, LKB1^{K78I}-, and LKB1^{D194A}-expressing DU145 cells. **(L)** Representative Western blot analysis for LKB1, p-AMPK, p-ACC, p-Raptor, Raptor, and HSP90 protein expression in control and LKB1^{WT}-, LKB1^{K78I}-, and LKB1^{D194A}-expressing DU145 cells (n = 5). **(M)** Western blot analysis of LKB1 protein expression in harvested xenograft tumors (n = 5 samples per condition). **(N)** Effect of LKB1 reconstitution in DU145 cells with ectopic expression LKB1^{WT}, the kinase-defective mutants (LKB1^{K78I}, LKB1^{D194A}) or infected with mock vector (pBABE) on tumor weight (left). Representative picture of harvested tumors (right) in xenotransplantation experiments (n = 20 injections per condition). **(O)** Quantification (left) and representative image (right) of Ki67 staining in harvested xenograft tumors in control and LKB1^{WT}-, LKB1^{K78I}-, and LKB1^{D194A}-expressing DU145 cells. Statistic test: one-sample t test (I); one-tailed Mann–Whitney test (N and O). *, P < 0.05; ****, P < 0.0001. Error bars represent SD (C, E, and F) and SEM (I, J, N, and O).

Downloaded from http://rupress.org/jem/article-pdf/217/6/e20191787/1780008/jem_20191787.pdf by guest on 09 February 2026

Tables S1–S10 are provided online as separate Excel files. Table S1 shows the incidence of metastasis in indicated tissues in $Pten^{pc+/-}$ $Lkb1^{pc-/-}$ mice. Table S2 shows STK11 in primary tumors and metastasis (Armenia et al., 2018). Table S3 shows the incidence of primary prostate tumors and metastasis in patients with indicated LKB1 genomic status (Armenia et al., 2018). Table S4 shows the frequency of copy number alterations (Armenia et al., 2018). Table S5 shows the frequency of coexisting mutations with LKB1 deletion among the top genes with copy number aberrations in the metastatic specimens (Armenia et al., 2018). Table S6 shows the incidence of primary prostate tumors and metastasis in patients with indicated SIK3 genomic status (Armenia et al., 2018). Table S7 shows the incidence of primary prostate tumors and metastasis in patients with indicated LKB1 and SIK3 genomic status (Armenia et al., 2018). Table S8 lists differentially expressed genes in microdissected specimens from $Pten^{pc+/-}$ $Lkb1^{pc-/-}$ (G2) versus $Pten^{pc-/-}$ $Lkb1^{pc+/+}$ mice (G5). Table S9 shows interactome analysis of LKB1 using Flag immunoprecipitation. Table S10 shows the Universal Probe Library (Roche) primers and probes used in this study.

Downloaded from http://rupress.org/jem/article-pdf/217/6/e20191787/1780008/jem_20191787.pdf by guest on 09 February 2026